Journal of Hydrology 546 (2017) 28–43

Contents lists available at ScienceDirect

Journal of Hydrology

journal homepage: www.elsevier.com/locate/jhydrol

Research papers

Velocity and celerity dynamics at plot scale inferred from artificial tracing experiments and time-lapse ERT

Anna Scaini [a,b,*], Marine Audebert [c,d], Christophe Hissler [a], Fabrizio Fenicia [e], Laurent Gourdol [a], Laurent Pfister [a], Keith John Beven [b,f]

[a] Luxembourg Institute of Science and Technology (LIST), Environmental Research and Innovation Department (ERIN), Catchment and Eco-Hydrology Research Group (CAT), L-4422 Belvaux, Luxembourg
[b] Lancaster Environment Centre, Lancaster University, Lancaster LA1 4YQ, UK
[c] National Research Institute of Science and Technology for Environment and Agriculture (IRSTEA), HBAN Research Unit, 1 rue Pierre Gilles de Gennes, CS 10030, 92761 Antony Cedex, France
[d] Sorbonne University, UPMC Univ Paris 06, UMR 7619 METIS, F-75005 Paris, France
[e] Eawag, Swiss Federal Institute of Aquatic Science and Technology, 8600 Dübendorf, Switzerland
[f] Geocentrum, Uppsala University, Uppsala, Sweden

ARTICLE INFO

Article history:
Received 5 September 2016
Received in revised form 25 October 2016
Accepted 21 December 2016
Available online 24 December 2016
This manuscript was handled by L. Charlet, Editor-in-Chief, with the assistance of WeiCheng Lo, Associate Editor

ABSTRACT

The relationship between tracer velocities and wave or wetting front celerities is essential to understand water flowing from hillslopes to the stream. The connection between maximum velocity and celerities estimated by means of experimental techniques has not been explored. To assess the pattern of infiltrating water front and dominant flow direction, we performed sprinkling experiments at a trenched plot in the Weierbach catchment in Luxembourg. Maximum velocities and wetting front celerities were inferred at different depths using artificial tracers, soil moisture measurements (TDR), and geophysical techniques. The flow direction was predominantly vertical within the observed plot, with almost no lateral flow observed until depths of 2–3 m; shallow trench flow was intermittent and associated with preferential flow. Average celerity estimates using TDR and geophysical techniques were equal to 707 ± 234 mm h^{-1} and 971 ± 625 mm h^{-1}, respectively. Vertical maximum velocity estimates were tracer-dependent and had very variable ranges: 109.3 ± 89.3 mm h^{-1} (Cl^-), 177.8 ± 199.1 mm h^{-1} (Br^-), and 604.1 ± 610.7 mm h^{-1} (Li^+). Preferential flow processes were inferred from maximum velocities apparently greater than celerities and scattered trench flow with highly variable tracer concentrations. The high variability between maximum velocities of different tracers indicated a complex pattern of tracer movement through the soil, not captured by celerity values alone. Our study demonstrated the importance to assess both velocities and celerities to understand flow dynamics in response to sprinkling while information on the wetting front alone would have missed important preferential flow processes.

1. Introduction

Spatial and temporal heterogeneity of soil and bedrock structure is known to control subsurface response, that often dominates runoff generation (Graham et al., 2010; McDonnell et al., 2007; Zehe and Sivapalan, 2009). Particularly in the unsaturated zone, the behaviour of the small-scale hydrological processes is highly nonlinear both temporally (wetting and drying phases) and spatially (Beven, 2012). Despite its proven importance, many unknowns still need to be resolved to improve understanding of such heterogeneity, in terms of how it affects water travel time characteristics as well as hydrograph responses (Botter et al., 2010; Rinaldo et al., 2011).

Travel time distributions are controlled by water velocities and filled pore space (Kirchner, 2016; Rinaldo et al., 2011). Conversely, the hydrograph response is controlled by celerities of the pressure responses and the effective storage that is filled and emptied as the wetting front progresses into the soil and the water tables rises and falls (Beven, 2010; McDonnell and Beven, 2014). One way to learn about the bulk effects of heterogeneities in the unsaturated zone at the hillslope and catchment scales is the interpretation of tracer observations to provide information about velocity distributions (Rinaldo et al., 2011) and simultaneous derivation of celerities from water content, piezometer and discharge responses (McDonnell and Beven, 2014).

* Corresponding author at: Luxembourg Institute of Science and Technology (LIST), Environmental Research and Innovation Department (ERIN), Catchment and Eco-Hydrology Research Group (CAT), L-4422 Belvaux, Luxembourg.
E-mail address: anna.scaini@list.lu (A. Scaini).

http://dx.doi.org/10.1016/j.jhydrol.2016.12.035
0022-1694/

McDonnell and Beven (2014) recently stressed the importance of characterising both tracer velocities, the measure of how fast pore water moves, and celerities, the measure of how fast the storage of water responds to a perturbation, in response to a rainfall event. This is critical as it helps explain the old-water paradox where streams can respond quickly to rainfall inputs but with water that has resided in the catchment for weeks, months or years (Beven, 1989; Kirchner, 2003). Beyond increased process understanding, the characterisation of velocities and celerities at the plot scale is necessary to implement physically reasonable model interpretations of flow at the larger hillslope and catchment scales.

Because of their nature, we expect velocity and celerity distributions to differ from each other, converging to similar values only in preferential flow domains (Hrachowitz et al., 2016). The differences between velocity and celerity are notions currently employed in the most novel modelling frameworks (Davies et al., 2013, 2011; Hrachowitz et al., 2013; Laine-Kaulio et al., 2014) and recent work showed the importance of experimentally derived tracer velocities in the spatial and temporal evolution of stream flow (Benettin et al., 2015; Bergstrom et al., 2016). Getting velocities and celerities right would mean that process representations are more likely to be, in the words of Kirchner (2006), right for the right reasons (see also Beven, 2010; McDonnell and Beven, 2014).

Sprinkling is the most widely used tool to control irrigation characteristics (Valipour and Singh, 2016; Valipour, 2012). In hydrological studies, sprinkling experiments carried out at trenched hillslopes are often used to characterise the vertical and lateral components of flow reaching different soil layers (McGlynn et al., 2002; Wienhöfer et al., 2009), allowing rainfall characteristics and, in part, boundary conditions to be controlled (McDonnell et al., 2007; Wienhöfer and Zehe, 2014). A recent sprinkling experiment showed the importance of the characterisation of multi-tracer approaches to estimate pore velocities, in an effort to characterise interflow and preferential flow (Jackson et al., 2016).

The observation of water flow is often combined with the detection of tracers, either natural, or artificial to quantify velocities. Chloride and bromide are amongst the most commonly used tracers to characterise water pathways (Graham and McDonnell, 2010; Perkins, 2011; Tyner et al., 2007). Bromide and lithium are considered to be near "ideal" tracers due to their very low natural abundance and relatively conservative characteristics (Flury and Papritz, 1993; Nickus, 2001). The interpretation of the tracer results may not, however, be simple. For example, suction lysimeters (Wagner, 1962) can be used to detect tracer arrival times (velocities) (Perkins et al., 2011), but the concentrations detected are expected to be a mix of mobile and relatively immobile water (Weihermüller et al., 2005). Additionally, geochemical processes, such as sorption/desorption, and root uptake effects will also affect measured concentrations (Weihermüller et al., 2007).

Soil moisture estimated using Time Domain Reflectometry (TDR) (Topp et al., 1980) can be used to detect the arrival of a wetting front (Haga et al., 2005), and some versions of the TDR probes can be used to infer electrical conductivity data as an indication of tracer arrival (Dalton et al., 1984; Persson, 1997). As wetting fronts can be highly spatially variable, obtaining spatially highly resolved data with point measurements using TDR remains challenging and expensive (Vereecken et al., 2014).

Electrical resistivity tomography (ERT) is a non-intrusive technique that can be used to provide spatially-resolved resistivity measurements of the subsurface (Binley and Kemna, 2005; Cassiani et al., 2006; Dahlin, 2001; Loke and Barker, 1996). Time-lapse surveys have been employed to characterise subsurface infiltration of water using the addition of tracers (Cassiani et al., 2009; Park, 1998; Slater et al., 2002), providing spatially and temporally resolved information on the wetting front.

The aim of this study is to explore the velocity and celerity responses at the plot scale, in a catchment where subsurface flows are known to contribute to riparian zone wetness and streamflows. Previous research in the Weierbach catchment has focused on identifying the dominant runoff generation processes (Fenicia et al., 2013; Wrede et al., 2015). Preliminary physiographic and geophysical investigations concluded that the fast drainage of the soil in addition to the relatively steep slopes generated lateral flow components in the subsurface and fractured bedrock (Wrede et al., 2015). However, the small-scale processes that are responsible for the hydrological response at catchment scale remain poorly understood.

Although the characterisation of velocities and celerities is important to infer flow pathways and residence times, how to best design experiments or this purpose is still poorly understood. This study examines downslope lateral flow in the soil profile (including preferential flow and patterns of local saturation), which previous experimental designs in the Weierbach catchment had not been able to track. Here, a three-fold monitoring protocol is designed for determining maximum velocity and celerity at plot scale. Installed on a trenched hillslope, the experimental set-up consists of [i] artificial tracers, [ii] time domain reflectometry (TDR), and [iii] geophysical techniques. In the framework of controlled sprinkling experiments, the complementarities and limitations of each of these techniques are explored – geared towards the estimation of maximum velocities and celerities within a schist plot.

2. Description of the experimental field site

The Weierbach, an experimental site located in the North-West of Luxembourg, has been monitored for its hydro-climatic response for more than 20 years. The catchment has an area of 0.45 km^2, is predominantly forested, and it is underlain by Devonian slate. The altitude ranges from 422 to 512 m a.s.l.

Within this catchment, a 64 m^2 plot has been isolated and instrumented (Fig. 1). The site is located on a north facing slope, on the left bank, just uphill of a forest road cut, 40 m from the river (Fig. 1a). The slope averages 10° and is perpendicular to the stream. At this location, the regolith consists of three main layers, which developed from periglacial slope deposits on the fresh Devonian slate bedrock (Juilleret et al., 2011, 2016).

The soil is classified as a Dystric Endoskeletic Cambisol (Colluvic, Bathyruptic, Siltic) in the WRB (IUSS Working Group WRB, 2015). From 0 to 40 cm depth, the soil has developed from a loamy material originated from periglacial slope deposits. It is divided in an upper thin organic rich A horizon (0–8 cm depth) and a cambic B horizon (8–40 cm depth). From 40 to 110 cm, the C horizon is composed of periglacial deposits dominated by slate rock fragments. At about 110 cm a lithic discontinuity occurs, separating the upper periglacial cover bed from the slate rock substratum. The deeper layer, from 110 to 500 cm depth, is constituted of weathered and fractured slate. The nearly vertical fractures, which are gradually closing with depth, permit rooting and, despite the impervious properties of the slate lithology, water can infiltrate through it. According to Martínez-Carreras et al. (2016), the mean drainage porosity decreases from the soil surface to the regolith-bedrock interface: 75%, 65% and <9% for the A, B and C horizons, respectively.

3. Materials and methods

3.1. The sprinkling experiments

Celerity and velocity depend on input intensity and antecedent conditions (Beven, 2012). Two sprinkling experiments were

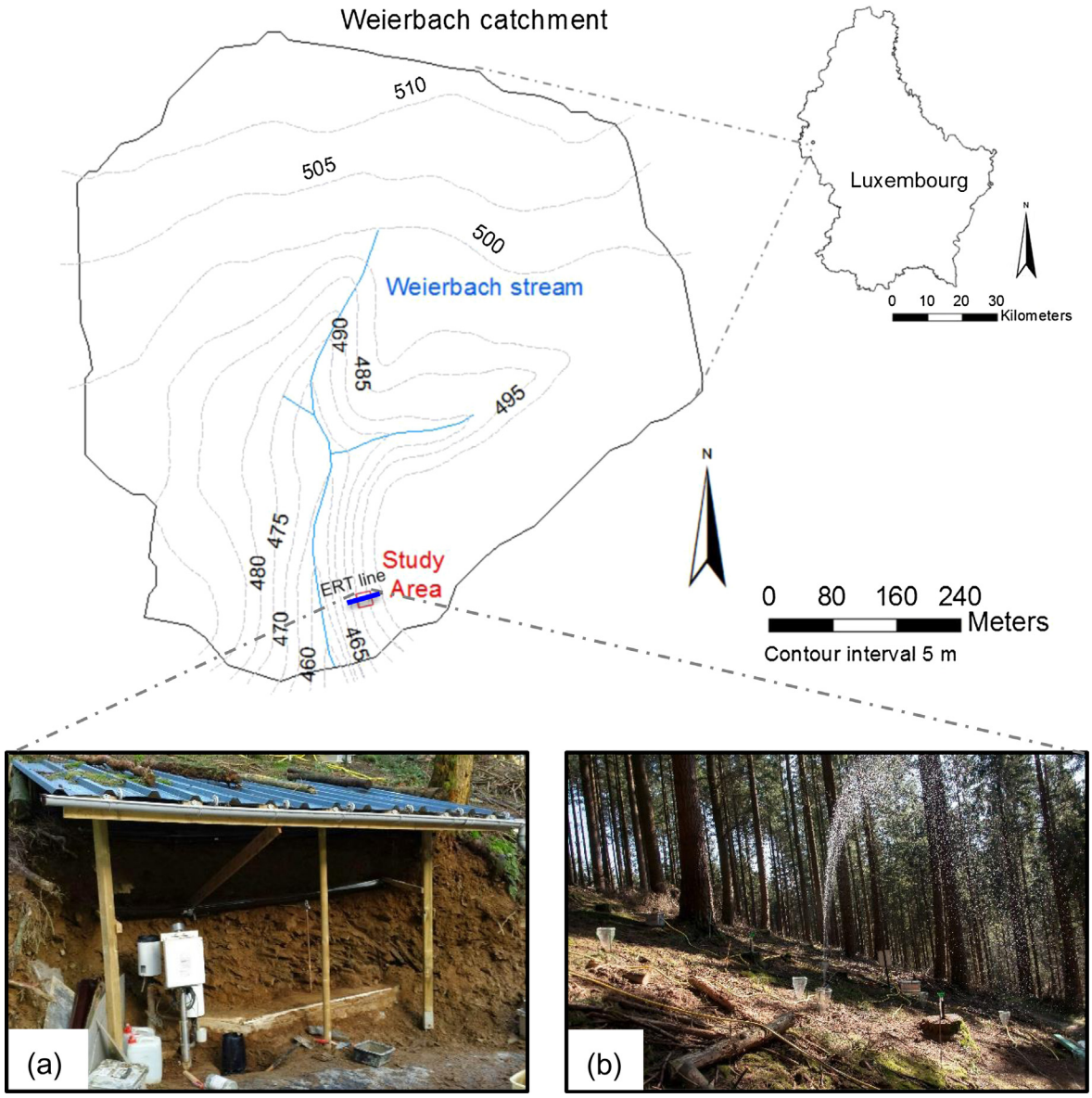

Fig. 1. Location of the Weierbach catchment, in Luxembourg. The plot is indicated by a red square. A blue line delineates the location of the ERT transect. (a) View of the trenched hillslope equipped with three sets of gutters and tipping buckets and protected by a roof; (b) side-view of the plot while sprinkling. (For interpretation of the references to colour in this figure legend, the reader is referred to the web version of this article.)

conducted under similar conditions of wetness. Intensity rates were kept as homogeneous as possible, in order to estimate maximum velocities and celerities and under comparable conditions.

3.1.1. Site implementation

Two garden sprinklers Gardena AquazoomTM 250/2 were used to perform artificial rainfall experiments, with the objective to apply water as uniformly as possible onto the plot surface. Rainfall intensities and uniformity were assessed by two types of water collectors. Permanent rainfall collectors were placed at 9 locations within the plot (Fig. 1b). During the sprinkling, 7 additional rainfall collectors were used to characterise more accurately the uniformity of the sprinkled water on the surface. Rainfall was measured at hourly time steps during the experiments. Rainfall intensities were derived from the spatial averaged value of the collectors. A summary of the sprinkling experiments is shown in Table 1.

The stream water of the Weierbach was used for the irrigation of the plot. This water presents a low mineralization level (electrical conductivity (EC) around 50 $\mu S\ cm^{-1}$) and its chemical composition did not interfere with the artificial tracing experiments. The natural background concentration of the tracers used during the experiment was estimated using data collected bi-weekly over a three year period (2011–2013) before the two experiments.

TDR sensors were used to measure the soil volumetric water content (VWC), before, during and after the sprinkling events. Changes in soil moisture and movements of the wetting front were estimated with 5 water content reflectometers (WCR – CS616, Campbell Scientific, 2011 Ltd.). The sensors were installed horizontally at 10 cm depth and vertically between 50 and 80 cm depth (Fig. 2). Additionally, a multi-parameter WCR sensor (CS650, Campbell Scientifics Ltd.) was installed vertically at the middle of the plot at 50–80 cm depth. It recorded EC and soil VWC. All sensors were connected to a CR10X datalogger (Campbell Scientifics Ltd.) for continuously recording soil VWC, temperature and EC at 15 min intervals.

Suction lysimeters (PTFE/Quartz – SDEC France) were inserted horizontally at 10 cm depth or vertically below the deeper WCR, at a depth of 80 –90 cm. The suction lysimeters allowed the soil

Table 1
Summary of irrigation for Experiment 1 and Experiment 2. Information of times (dates, number of sprinkled days), antecedent conditions (API = antecedent precipitation index, calculated for a 30 and 7 days period before the experiment (in brackets); AMC = antecedent moisture conditions, at two depths in the soil); total irrigation (mm) measured over an area of 64 m^2; quantity of tracers applied.

Experiment	1	2
Dates	31/03–10/04 2014	11–16/03/2015
Days of sprinkling	9	6
API 30 [7] (mm)	12 [0.9]	50 [8]
AMC 10 cm depth ($cm^3\ cm^{-3}$)	0.23	0.27
AMC 50–80 cm depth ($cm^3\ cm^{-3}$)	0.40	0.35
Total irrigation (mm)	573.3	352.9
Tracers applied (kg) [$g\ L^{-1}$]		
NaCl	25 [5]	5 [5]
KBr	5 [2.5]	
LiCl		2.5 [1]

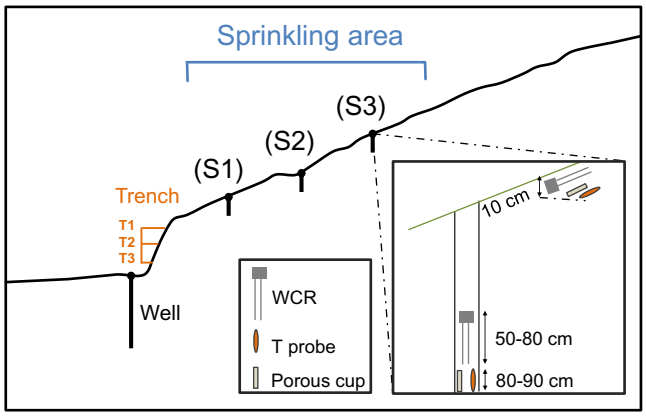

Fig. 2. Description of the experimental equipment. In the box, view of the WCR, temperature probes and porous cup inserted horizontally at 10 cm depth and vertically between 50 and 80 cm depth in each of the three soil pits (S1, S2 and S3). The trench position, including the three gutters (T1, T2, T3) is shown in orange. (For interpretation of the references to colour in this figure legend, the reader is referred to the web version of this article.)

solution that drained the soil during the infiltration experiments to be sampled at variable time step (between 30 min and 3 h) in order to determine the evolution of the artificial tracer concentrations.

In order to collect shallow subsurface water flow, a 350 cm long trench was excavated at the downstream part of the experimental site (Fig. 1a). Through the trench, 3 lateral flow troughs of 150 cm length were inserted. They were used to conduct the outflow from the trench at 25, 50 and 130 cm depth to collection points, equipped with a volume collector and a tipping bucket rain gauge (Model 52203, Young). The number of tips recorded by the tipping buckets was then converted to volume of shallow lateral flow at a 5 min time step. The sensors were connected to a DRX10 datalogger (Campbell Scientifics Ltd.).

In order to capture deeper lateral flow, two wells were installed at the base of the trench. The drilling was performed from the surface of the forest road, on the two sides of the roof covering the base of the plot. The two wells were drilled at 2 and 2.4 m depth and went through the fractured slate layer. Both wells were equipped with OTT Thalimedes probes to measure water height, temperature and EC at 1 min time step.

3.1.2. Sprinkling experiment 1

The goal of the sprinkling experiment was to generate heavy rainfall conditions, which would trigger lateral flow. The first sprinkling experiment was conducted in two steps between the 31st March and 10th April 2014 separated by a two days period (April 5th and 6th) without sprinkling. Meteorological conditions prior to the experiment were relatively dry: the antecedent precipitation index (API) was equal to 12 mm for a 30 days period before the experiment (API30) and 0.9 mm for a period of one week prior the experiment (API7) (Table 1). The antecedent moisture content, calculated as the mean daily value of the WCR probes, was 0.23 $cm^3\ cm^{-3}$ at 10 cm depth and 0.40 $cm^3\ cm^{-3}$ at 50–80 cm depth. During step 1, only one sprinkler was used and mean intensities ranged from 7.6 to 11.4 mm h^{-1}, depending on wind and cleanliness of the sprinkling system. Since no trench flow was measured, a second sprinkler was used during step 2 and contributed to rise the applied intensity up to 20.5 mm h^{-1} (Table 2). The total rainfall volume sprinkled over the first experiment was equivalent to 573 mm (a total of 36,700 L).

During the sprinkling experiment, on Day 3 and Day 8 (April 2nd and 9th – Table 1), a tracer solution of respectively 3000 and 2000 L with 5 g L^{-1} NaCl was used to sprinkle the area. On Day 9 (April 10th), a solution of 2000 L with 2.5 g L^{-1} KBr was applied.

The first NaCl application (Day 3) had as primary objective the assessment of the wetting front with time-lapse ERT in combination with the *in-situ* probes, ultimately needed to measure celerity response. Adding tracer to the sprinkled water was necessary to estimate maximum velocities by detecting the tracer arrival from the chemical composition of sampled water at each measurement point. The *in situ* probes could characterise point-based celerity information for each sprinkling day. The later applications had the objective of characterising the movement of water through the soil with different tracers, to account for their differences.

3.1.3. Sprinkling experiment 2

Experiment 2 (Table 1) was conducted in March 2015, in order to replicate the wetting phase and using a new salt, LiCl. The sampling interval for the suction lysimeters was reduced up to 1 h to give a better definition of the evolution of the artificial tracer concentrations.

In terms of antecedent conditions, API30 was equal to 50 mm (API7 = 8 mm), about 4 times higher than in Experiment 1. The average VWC was 0.27 $cm^3\ cm^{-3}$ at 10 cm depth and 0.35 $cm^3\ cm^{-3}$ at 90 cm depth respectively, and did not differ significantly from Experiment 1. The hillslope was sprinkled with intensities as similar as possible to Experiment 1 (step 2) for a total of 6 days, with a total irrigation of 353 mm (equal to 22,600 L). Two tracers were applied on Day 3 of Experiment 2 (13/03/2015): a solution of 1000 L containing 5 g L^{-1} NaCl and one of 1000 L containing 1 g L^{-1} LiCl were used. NaCl was employed again in order to compare estimates of celerities of Experiment 1 and 2 using the same tracer.

3.1.4. Chemical analyses of tracers in the soil

During both experiments, soil solution samples were taken [i] using the suction lysimeters at 6 different locations in the soil and [ii] at the volume collectors placed at each trough exit (Fig. 2). All collected water samples were filtered at 0.45 μm using Acrodisc syringe filters (Pall Corporation) before analysis of EC, chloride (Cl^-), bromide (Br^-) and lithium (Li^+) concentrations. The concentrations were analysed using ionic chromatography (Dionex ICS-5000). The detection limit of the analyses was 0.01 mg L^{-1} for Cl^-, 0.02 mg L^{-1} for Br^- and Li^+. Tracer recovery at the trench face was calculated with input-output rate estimation. For each collected sample from the suction lysimeters and trench, the quantity of tracer with respect to the input concentration (respectively equal to 6.3 g L^{-1} for Cl^-, 5.2 g L^{-1} for Br^-, 0.3 g L^{-1} for Li^+) was also calculated.

EC measured with the multi-parameter WCR sensor is widely employed as a proxy value for ion concentration (as largely used in field studies, see McNeil and Cox, 2000; Siosemarde et al.,

Table 2
Sprinkling rates according to the sprinkling set-up: (a) Experiment 1, step 1, using one sprinkler; (b) Experiment 1, step 2, using 2 sprinklers: (c) Experiment 2, using 2 sprinklers. Total rainfall, Total time sprinkling and mean intensity are shown. **Bold**: days of artificial tracer application.

	Date	Total rainfall (mm)	Total time sprinkling (h)	Mean intensity (mm h^{-1})
a	31/03/2014	30.5	4	7.6
	01/04/2014	76.4	7	10.9
	02/04/2014	69.4	6.5	10.7
	03/04/2014	22.8	2	11.4
	04/04/2014	32.7	3	10.9
b	07/04/2014	37.9	3	12.6
	08/04/2014	86.4	5	17.3
	09/04/2014	123.2	6	20.5
	10/04/2014	91.8	6	15.3
c	11/03/2015	36.9	3	12.3
	12/03/2015	92.3	6	15.4
	13/03/2015	72.3	6	12.0
	14/03/2015	64.9	5	13.0
	15/03/2015	48.4	4	12.1
	16/03/2015	37.5	3.5	10.7

2010). Since different tracers were employed, a correlation equation between EC and the tracers could not be generated, but the EC trend was used to assess tracer dynamics at that location.

3.2. Monitoring infiltration using time-lapse ERT

The ERT method is widely described in the geophysics literature and used to study subsurface variations in electrical resistivity linked with variation of water content, clay content, porosity, saturation and the concentration of dissolved electrolytes (Dahlin, 2001; Loke and Barker, 1996; Telford et al., 1990; Tsourlos and Ogilvy, 1999). Compared to standard ERT, time-lapse ERT can provide information on the time variability of electrical resistivity. Time-lapse ERT monitoring involves performing identical ERT surveys several times at the same location (Daily et al., 1992), for example before, during and after the sprinkling experiment. Salt tracer injection implies an increase in electrical conductivity and consequently a corresponding decrease in electrical resistivity. Time-lapse surveys demonstrated the high potential for monitoring water infiltration during rain experiments (Descloitres et al., 2008; Travelletti et al., 2012).

However, two main limitations of the ERT method can be identified: [i] the non-uniqueness of the inversion process, meaning that multiple spatial reconstructions of the resistivity may be consistent with the observations, and [ii] the smoothness-constrained regularisation method, which tends to smooth the resistivity models creating difficulties to locate the infiltration front precisely. To overcome these issues, several strategies for ERT interface detection have been developed (Chambers et al., 2014; Nguyen et al., 2005; Ward et al., 2014). In another study, Audebert et al. (2014) developed the multiple inversions and clustering strategy (MICS) to better delineate the infiltration area on time-lapse ERT monitoring data sets. The methodology was assessed on numerical data and leachate recirculation field data. For the first time, this methodology was used in a hydrological study, in order to delineate infiltration at the plot scale.

3.2.1. ERT transect

The ERT transect used in this experiment features 120 electrodes with an electrode spacing of 0.5 m. The ERT survey location is represented by a blue line in Fig. 1. The alignment of the electrodes follows the direction of the main slope gradient and the centre of the electrode line was located just above the upper limit of the sprinkling area. Precise location of each electrode was determined using a Trimble DR3300 Total station. The ERT measurements during tracer injection experiments were conducted with a Syscal Pro 120 (ten-channel) resistivity meter from IRIS instruments. A Wenner-Schlumberger quadripole array configuration was used for the measurements due to its good depth of investigation and spatial resolution (Athanasiou et al., 2007; Dahlin and Zhou, 2004).

3.2.2. The multiple inversions and clustering strategy (MICS)

The MICS methodology is based on two steps:

i. A multiple inversion step to take into account the variability of the inversion process in varying inversion parameters. In this paper, inversions of time-lapse ERT data sets were performed to reconstruct the resistivity distributions using the Boundless Electrical Resistivity Tomography code (BERT) from Günther et al. (2006). To determine the misfit between simulated and field data sets of apparent resistivity, the classical inversion tools use the root mean square error (RMSE) (Loke and Barker, 1996) and the Chi^2 mathematical criteria (Günther et al., 2006). The resistivity models exhibiting a RMS higher than 5% were discarded.
ii. A clustering strategy, based on a grouping criteria, to classify the results in delineating the infiltration area on the final profile (Audebert et al., 2014). In the original paper Audebert et al. (2014), the grouping criteria was based on the following rule: if a mesh cell belongs to the infiltration area for all clustering profiles (100% of belonging), this cell belongs to the infiltration area in the final profile. This stringent criterion of 100% would allow greater confidence in the delimitation of the area of infiltration, however retaining part of the information. This criterion was therefore relaxed and the % of times that each mesh element belonged to the infiltration area was computed using 4 grouping criteria with 60%, 70%, 80%, 90% belonging thresholds.

On the basis of previous MICS numerical tests (Audebert et al., 2014), a total of 32 inversions is required for each resistivity data set. Sensitivity was computed for each inversion parameter set and data interpretation limited to the smallest high-sensitivity area among all the inversion results (Audebert et al., 2014). The MICS methodology was applied to the four ERT data sets recorded before and during the tracer injection experiment, requiring a total of 128 inversions.

3.3. Estimating celerity and maximum velocity from the sprinkling experiments

Fig. 3 shows a conceptual illustration of the response of a 1-D non-confined system to a water input. Fig. 3a shows the traced

water input. The water input creates a wetting front moving in the vertical direction, which displaces some of the particles of water already stored in the soil (Fig. 3b). In such system, the maximum velocity is defined as the fastest direct movement of the tracer. There is an expectation that the wetting front response will be faster than the tracer responses as a result of the celerity being faster than the water velocity (Fig. 3c1). On some occasions, bypassing or preferential flow might occur, limited by the speed of the fastest (maximum) velocity. Only in this case, where tracer moves ahead of the main wetting front, will the maximum velocity therefore appear as higher than the wetting front (celerity) (Fig. 3c2). For the maximum velocity to be higher, tracer would need to be detected in the suction lysimeters (sampled at smaller intervals) before detecting any change in the moisture content, either due to preferential flow missing the TDR probe or within the uncertainty of MICS.

The celerity was calculated for each sprinkling day using the time of the first response of VWC and trench flows to sprinkling, respectively measured by TDR probes and tipping buckets. The overall response of the plot was described by showing a range of values, due to the time-range of the measurements. The celerity of the wave response was estimated dividing the depth of the probe by the time lag between start of irrigation and response of the probe. The probes inserted vertically in the hand dug soil pits are expected to respond as soon as the upper part of the probe is wetted. The values of celerity were calculated as a range from minimum (50 cm depth) to average depth of the probe (65 cm depth).

The maximum velocity was calculated using the artificial tracer concentrations measured in the soil water samples collected in the suction lysimeters, and from the arrival time of the tracers at the trench face. In case of the suction lysimeters, the values are given as ranges due to the coarser sampling interval (Section 3.1.1). In the case of the suction lysimeters inserted vertically in the hand-dug soil pits, the values of maximum velocity were calculated over the average depth of the probe (85 cm depth). The timing of the sharp rise in concentration following the addition of tracer provides the estimate of maximum velocity, but might miss any preferential flow occurring in between sampling time-steps.

The maximum velocities estimated for the sprinkling days were directly compared with the correspondent celerities for the same days.

3.4. Estimating celerity from MICS

Wetting front celerities were calculated from the depths of the infiltration delimited with MICS and for each of the 4 grouping criteria (Section 3.2.2). Celerities were computed considering the topographic position of the three VWC profiles (positions corresponding to S1, S2 and S3 in Fig. 2) at different times. MICS celerity was computed at the correspondent location in the ERT profile. The maximum depth reached is divided by the elapsed time, corresponding to the time interval of the three ERT data sets, recorded respectively 70, 175 and 280 min after start of salt sprinkling.

3.5. Estimating apparent porosity

The ratio between the injected volume of water and the infiltration volume delimited by MICS at each time step, ε_a, defined as "apparent porosity" by Clément et al. (2011) and Audebert et al. (2016), provides an estimate of the pore volume used for water flow. In the first part of their study, Audebert et al. (2016) showed that a small value of ε_a (between 3% and 9%) implies that a very small fraction of the pore volume is available for water flow, which could be interpreted as fast and possibly preferential flow pathways.

4. Results

4.1. Trench flow and velocity/celerity estimates

During Experiment 1, the relative amount of lateral flow reaching the trench, was a total of only 24 L, equivalent of a 0.03% of the total input sprinkled onto the experimental plot surface. The lateral connectivity, i.e. trench flow, was reached only on the last 3 sprinkling days of Experiment 1. A larger precipitation rate than initially applied (on average between 15 and 28 mm h^{-1}) was necessary to generate lateral connectivity and initiate trench flow. Cl^- was used in 3 different occasions, and its interpretation in terms of response at the trench face is complicated due to the non-activation of the trench during the first part of Experiment 1. Therefore, Cl^- data were not included in the analysis.

On Day 9, April 10th, T1 and T2 were activated by water sprinkled prior to the salt experiment, with estimated celerity of respectively 1000, 166 and 90 mm h^{-1}. Before applying the KBr solution, the flow at T1 and T2 slowed down due to a 20 min break in the irrigation. Only after 20 min of sprinkling the salt solution, both T1 and T2 flow increased again, allowing a second estimate of celerity to be made of respectively 750 and 1500 mm h^{-1} (Table 3a). At T3, the first tip was recorded 4 hours after starting sprinkling on that day, and one hour after starting the tracing experiment (celerity of 1733 mm h^{-1}).

Similar results were observed during Experiment 2: only a total of 30 L flowed to the trench (0.08%), even though the trench was activated on each sprinkling day. During Experiment 2 (March 13th 2015), only T1 was activated with celerity of 63 mm h^{-1}. Sprinkling was continuous, but before sprinkling Li^+, filters were cleaned, and consequently the intensity was increased. Water reached T2 (with a celerity of 1000 mm h^{-1}), before T1 reactivation (celerity of 273 mm h^{-1}, see Table 3b).

The maximum velocities at the trench were estimated using the detection time of the applied tracers. During Experiment 1, Cl^- concentrations ranged between 9.30 and 1113.80 mg L^{-1} (T1), between 13.20 and 598.90 mg L^{-1} (T2), and between 4.20 and 260.90 mg L^{-1} (T3). Br^- concentrations ranged between 118.50 and 556.00 mg L^{-1} (T1), between 5.00 and 176.00 mg L^{-1} (T2), and between 0.50 and 133.00 mg L^{-1} (T3). Br^- reached T1 25 min after starting the tracer experiment and T2 after only 15 min (maximum velocities of respectively 600 and 1200 mm h^{-1}). During Experiment 2 Cl^- concentrations ranged between 6.00 and 96.00 mg L^{-1} (T1), and between 7.80 and 242.50 mg L^{-1} (T2). Li^+ concentrations ranged between 0.20 and 2.40 (T1) and were only equal to 0.02 mg L^{-1} (detection limit) in T2. On March 13th, 2015, Li^+ reached T1 30 min after start of sprinkling (maximum velocity of 517 mm h^{-1}) while it reached T2 only on the next day (maximum velocity of 17 mm h^{-1}). The chemical analysis on the volumes collected at the trench during Experiment 2 revealed that Br^- concentrations (used as tracer only during Experiment 1, see Table 1) were still high nearly one year later (0.70–30.00 mg L^{-1} Br for T1, 8.00–273.10 mg L^{-1} for T2).

4.2. Chemical evolution of soil water

Fig. 4 shows the time series of rainfall (Fig. 4a) and the multi-parameter probe placed in S2 at 50–80 cm depth (Fig. 4b). Both VWC and EC values (expressed as μS cm^{-1}) are shown, respectively in green and orange. The time series of EC monitored by the sensor in the soil matrix is characterised by 3 phases (Fig. 4b). The data recorded after Experiment 1 show peaks of EC correspondent to the peaks of VWC during rainfall events (Fig. 4b, Part 1). The higher value of EC during these peaks corresponds to 118.4 μS cm^{-1}, likely to be much higher right after Experiment 1. The magnitude of

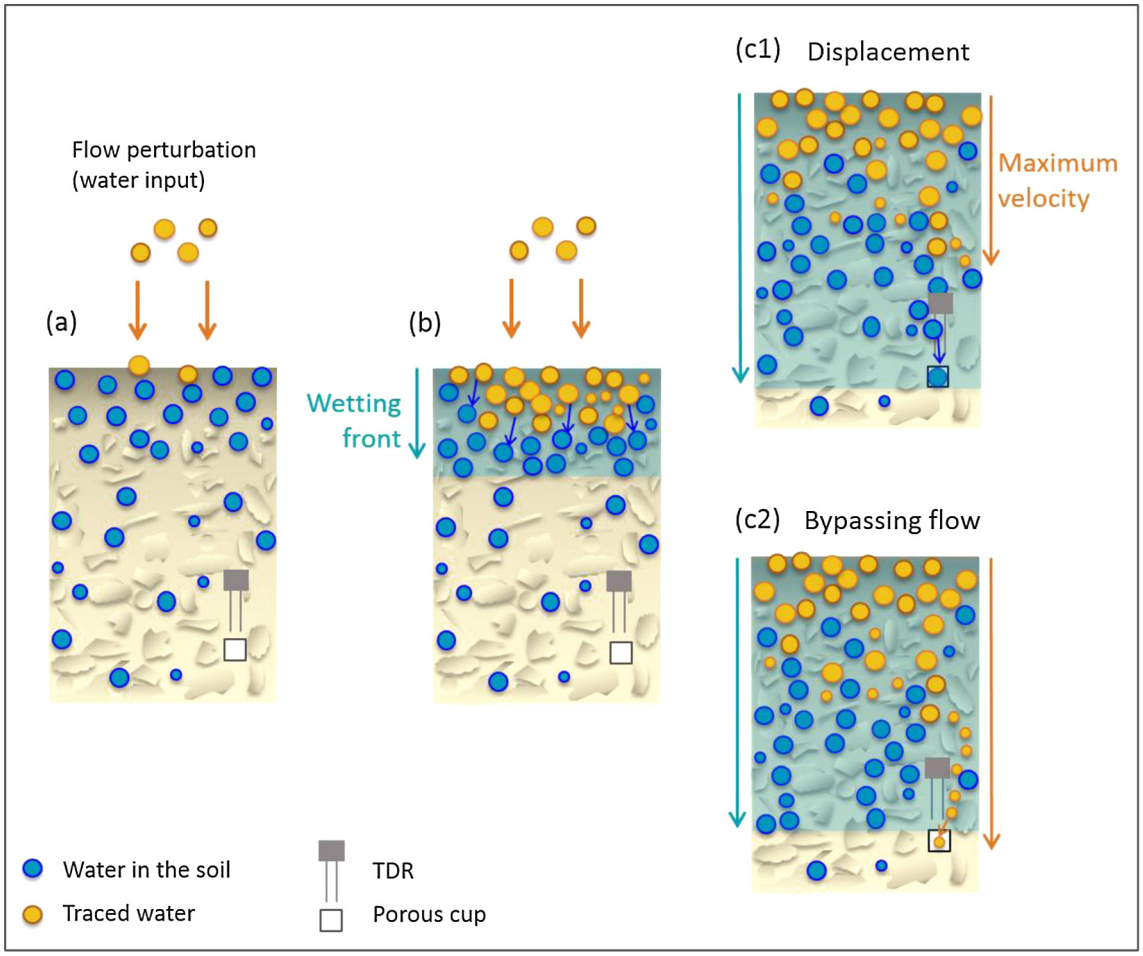

Fig. 3. One-dimensional sketch of a schematic soil box showing the difference between celerity and velocity estimated in this paper. The response to the sprinkling event using traced water (a) is shown. A wetting front is generated as a consequence to the pressure given by the water input (b). A process of displacement moves the water stored in the soil until reaching the measurement point (c1). Bypassing flow occurs when traced water moves through preferential flow reaching the measurement point in correspondence with, or even "before", the wetting front (c2).

Table 3
Celerities (a) and velocities (b) estimated at the trench expressed as mm h^{-1}. Each value of velocity refers to the detection of the tracers in the sampled water. Cl^- data are not included because of the difficulty in the interpretation. X = no data, meaning that there was no trench flow. Underlined: no data on that day – tracer reached on the next day.

Date	Precipitation (Tracer)	T1	T2	T3
a. Celerities (mm h^{-1})				
10/04/2014	P1	1000	166	90
	P2 (Br^-)	750	1500	1733
13/03/2015	P1	63	X	X
	P2 (Li^+)	273	1000	X
	Tracer	T1	T2	T3
b. Velocities (mm h^{-1})				
10/04/2014	Br^-	600	1200	918
13/03/2015	Li^+	517	17	X

these peaks got progressively smaller in the last part of 2014, until almost no fluctuation was present in early 2015 (Fig. 4b, Part 2). During Experiment 2, EC started with the lowest value of 21.5 µS cm^{-1} and raised again with the salt tracing, responding to the sprinkling with 15 min lag (one time step) with respect to the VWC probe (Fig. 4b, Part 3, and Fig. 4d). The magnitude of Experiment 2 peak had a maximum of 98.5 µS cm^{-1}.

Before Experiment 1, background EC of the soil water collected in the suction lysimeters at 65 cm depth was 152 µS cm^{-1}. The average background Cl^- value in the suction lysimeters was 3.23 ± 2.24 mg L^{-1} (no Br^- or Li^+ were detected in the samples). NaCl and KBr input water had EC values respectively of 9500 and 2300 µS cm^{-1}. During Experiment 1, EC in the water extracted from the lysimeters at 65 cm depth raised up to 1400 µS cm^{-1}. The samples collected using the suction lysimeters at 10 cm depth had concentrations of Cl^- up to 16.1% higher than those placed at 85 cm depth, and concentrations of Br^- up to 9.1% higher. Before Experiment 2, both Cl^- and Br^- concentrations were still high with respect to the initial background concentrations: 12.87 ± 5.18 mg L^{-1} for Cl^-, 7.48 ± 9.90 mg L^{-1} for Br^- at 10 cm

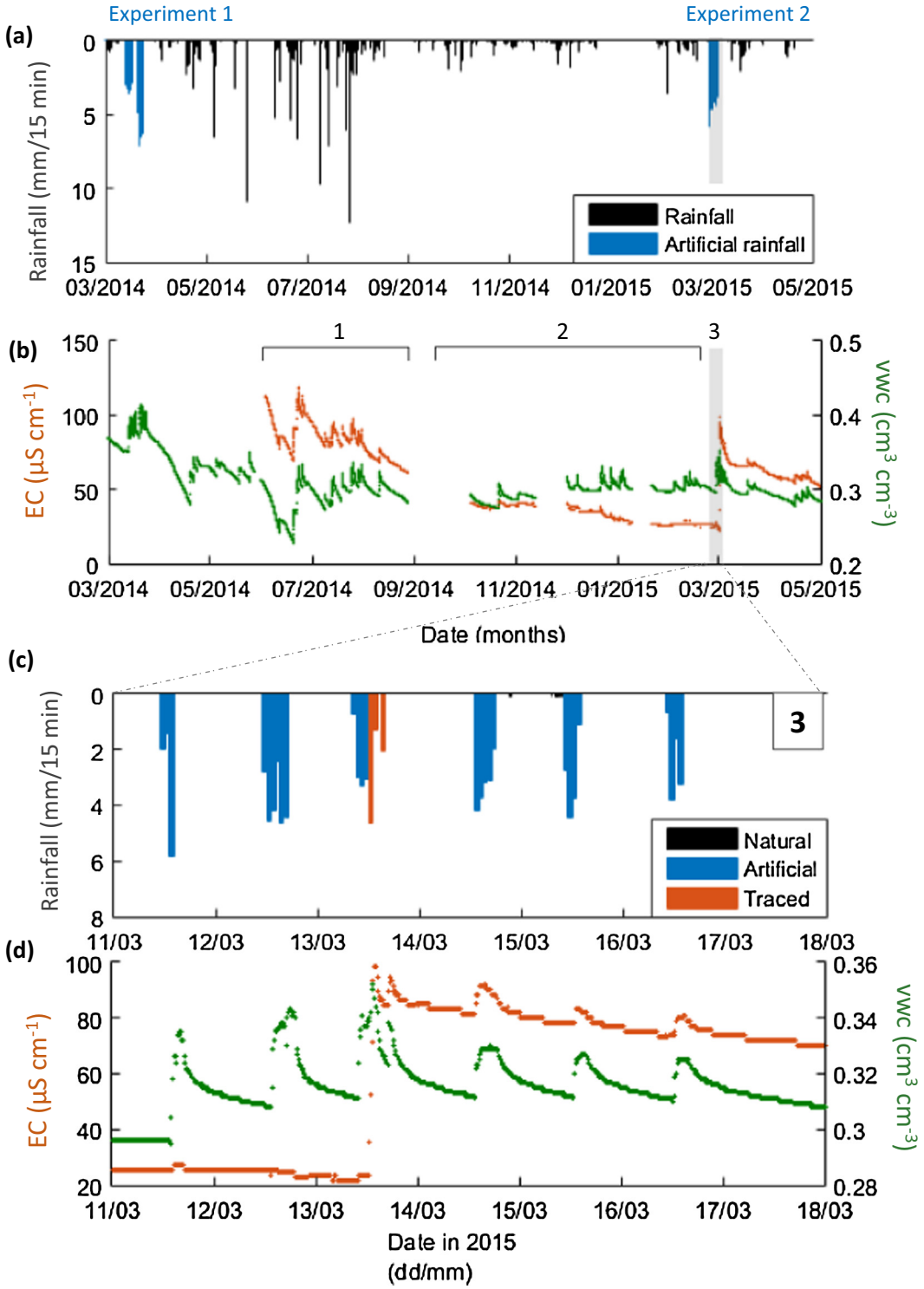

Fig. 4. Time series of (a) rainfall, (b) soil moisture, expressed as volumetric water content (VWC, green) and electrical conductivity (EC, orange) at S2, for the 50–80 cm depth. Three main periods are distinguished: (1) remobilization of the salt during natural rainfall events; (2) dilution of salt during natural rainfall events and (3) the effect of Experiment 2 on EC due to raise in salt concentration. Graphs (c) and (d) correspond to a zoom of period 3 and show the sprinkling sequence, VWC and EC response during Experiment 2. On Day 3, the EC rises again due to the salt solution sprinkled. (For interpretation of the references to colour in this figure legend, the reader is referred to the web version of this article.)

depth, 64.85 ± 31.48 mg L^{-1} for Cl^- and 31.60 ± 19.75 mg L^{-1} for Br^- at 85 cm depth. During the first days of sprinkling, no peaks in EC were recorded in the soil matrix (Fig. 4d). With Experiment 2, NaCl and LiCl input water had values of EC respectively of 9500 and 2600 µS cm^{-1}.

The tracer concentrations for each suction lysimeter, during both Experiment 1 (right graphs) and Experiment 2 (left graphs), are shown as box plots in Fig. 5. The full concentration range over the totality of the sprinkling days is shown for each of the suction lysimeters, with red lines indicating the median value. On the first

days of Experiment 2, before applying tracers, average concentrations on the plot were 37.00 mg L^{-1} Cl^- and 39.00 mg L^{-1} Br^- at 10 cm depth, 52.00 mg L^{-1} Cl^- and 28.00 mg L^{-1} Br^- at 85 cm depth. During Experiment 2, Cl^- concentrations in the suction lysimeters ranged between 8.20 and 770.00 mg L^{-1}. Li^+, sprinkled on March 13th, was detected in all the suction lysimeters, and its concentration ranged between 0.03 and 18.40 mg L^{-1}. Concentrations at 10 cm depth were up to 3.6% higher than 85 cm depth for Cl^-, and 0.2% for Li^+. During Experiment 2, Br^- was still detected at all locations. Its concentrations were very similar at both depths and ranged between 0.30 and 58.00 mg L^{-1} (Fig. 5).

4.3. Maximum velocity estimates

Fig. 6 shows estimates of maximum velocities calculated for the application of each tracer: April 02 (Cl^-) and 10 (Br^-), 2014 and March 13, 2015 (Cl^- and Li^+). Maximum velocities were always higher in the deeper probes on average by 4.0 ± 5.4% (Fig. 6). Cl^- maximum velocities were very similar in Experiment 1 and 2, with an average value of 36 ± 16 mm h^{-1} (shallow probes) and 127 ± 65 mm h^{-1} (deep probes) in Experiment 1 and 38 ± 14 mm h^{-1} (shallow probes) and 123 ± 87 mm h^{-1} (deep probes) in Experiment 2 (Fig. 6).

Even though Cl^- and Li^+ were applied on the same day during Experiment 2, their values of velocity were very different. Li^+ had the highest estimates of maximum velocity (Fig. 6): on March 13th, in S3 Li^+ reached the deep probe before the shallow probe at the same location, and almost simultaneously with the shallow probe of S2 and deep probe at location S1. Concurrently, maximum velocities were respectively 1282 ± 351 mm h^{-1} for deep probe S3 and 1260 ± 191 mm h^{-1} for deep probe S1 (Fig. 6). Li^+ reached deep S2 only on the overnight sample. Average Li^+ maximum velocities were 103 ± 68 mm h^{-1} and 677 ± 420 mm h^{-1} respectively for shallow and deep probes.

On April 10, Br^- was detected only in S3 (Fig. 6, blue) only 3–5 h after sprinkling, with maximum velocities of respectively 27 ± 10 mm h^{-1} (shallow probe) and 232 ± 83 mm h^{-1} (deep probe), but was detected in S1 and S2 only after a 2 days-long delay (data not shown). On Experiment 2, Br^- was present in all the suction lysimeters at all times and progressively diluted and was therefore not used for velocity calculations.

4.4. Celerity estimates

The estimates of celerity could be calculated from the VWC data. Averaged VWC for the three locations at same depth within the hillslope (S1, S2 and S3), plotted against the rainfall, are shown in Fig. 7. Fig. 7a presents both natural (in black) and sprinkled rainfall (in blue), expressed as mm/15 min. Fig. 7b shows the time series of VWC at 10 cm (orange) and 50–65 cm depth (green). Over the full time series, at 10 cm depth, the VWC ranged between 0.709 and 0.185 cm^3 cm^{-3}, while at 50–65 cm depth it ranged between 0.516 and 0.351 cm^3cm^{-3}, showing higher fluctuations in the shallow probes. Correlation between the probes (calculated for the full time series and only between probes at same depth) ranged between 0.80 and 0.89. Even if the API was higher before Experiment 2 by 38 mm (API30), the average VWC was higher before Experiment 1 by 5%.

Fig. 8 shows estimates of celerities at the plot scale calculated for the application of each tracer: April 2nd (Cl^-) and 10th (Br^-), 2014 and March 13th, 2015 (Cl^- and Li^+). Celerity values were always higher in the deep probes on average by 5.1 ± 2.3% (calculated from Fig. 8). Averaged values of celerities in Experiment 1 were respectively 420 ± 197 mm h^{-1} (shallow probes) and 747 ± 379 mm h^{-1} (deep probes) for April 2nd, and 579 ± 484 mm h^{-1} (shallow probes) and 1183 ± 448 mm h^{-1} (deep probes) for April 10th (Fig. 8). During Experiment 2, on March 13th 2015, celerities were significantly lower showing that at all locations water needed more time to reach the measurement points. Average celerities were respectively 84 ± 13 mm h^{-1} for shallow probes and 384 ± 85 mm h^{-1} for deep probes (Fig. 6).

4.5. Time-lapse ERT

This section focuses on Day 3 of Experiment 1, April 2nd, when the NaCl solution was sprinkled for the first time. Fig. 9 shows the time series of sprinkled rainfall (a) and VWC responses (b). The plot was sprinkled for 1.5 h (from 10 h 35 min to 12 h, indicated by P1 in Fig. 9a). After a stop of 2.5 h, the plot was sprinkled with the NaCl solution (P2, orange-coloured). The three time steps of time-lapse ERT following salt sprinkling are indicated by grey vertical lines: time steps b, c, and d (70, 175 and 280 min after the beginning of salt sprinkling, respectively).

4.5.1. Resistivity changes due to salt application

Fig. 10 presents the ERT results obtained during Experiment 1 of salt sprinkling. Profile (a) represents the initial interpreted resistivity (before the beginning of the salt sprinkling) and was obtained from a standard inversion procedure (i.e. L1-norm, w_z equal to 1 and a λ value of 20). The variability of resistivity with depth corresponds well with the regolith vertical structure as observed in the trench and core drillings of both wells. Resistivity in the first 0.5 m depth (A and B horizons) is around 1000 Ω m (light blue,[1] Fig. 10a). Between 0.5 and about 2.0–2.5 m depth, resistivity forms a sharp peak (yellow to red, Fig. 10a), with a maximum of 7000–10,000 Ω m at around 1.0–1.5 m depth. The increase in resistivity corresponds to the C horizon, whilst the decrease deeper in the profile corresponds to the first heavily fractured part of the bedrock. Resistivity progressively decreases to a minimum of 100–500 Ω m at 5 m depth, as bedrock becomes fresher (dark blue, Fig. 10a). The pre-sprinkling signal is therefore characterised by very low porosity and resistivity at deeper layers, due to the physical properties of the bedrock.

The values of resistivity obtained with the standard inversion of the initial ERT data set ensures that the resistivity contrast between the salt tracer solution used during Experiment 1 (conductivity of 9.5 mS cm^{-1}, corresponding to a resistivity of 1.1 Ω m) and the surrounding medium, will be high (particularly until 2.5 m depth where pre-sprinkling resistivity is high).

4.5.2. Using MICS to characterise water penetration depth

MICS results are presented according to grouping criteria between 30% and 100% (Fig. 10b, c and d). Each grouping criteria result is shown based on the colour ramp – from grey for areas that changed less than 60% of the times, to white, for intermediate values, and blue, assigned to the clustering result indicating the pixels that were changing in all the 32 inversions for each time step (100%). An infiltration plume based on the grouping criterion is therefore visible. In the upper part of the plot (S3), the plume of infiltration reaches 1.60 m (90%) to 2.25 m depth (70%) depending on the grouping criterion (Fig. 10b). The tracer infiltration expands in depth in the middle (S2) part of the plot (until 1.00–1.60 m) and partially in the downslope direction (Fig. 10c). Only on the third time step (Fig. 10d) does the plume reach a depth of 1.35–1.85 m in the bottom part of the plot (S1). The maximum depth is reached at location S3, with 1.95 m (90%) to 2.45 m depth (70%). No significant resistivity changes indicating infiltration are observable below 2.50 m.

[1] For interpretation of colour in Figs. 7, 9 and 10, the reader is referred to the web version of this article.

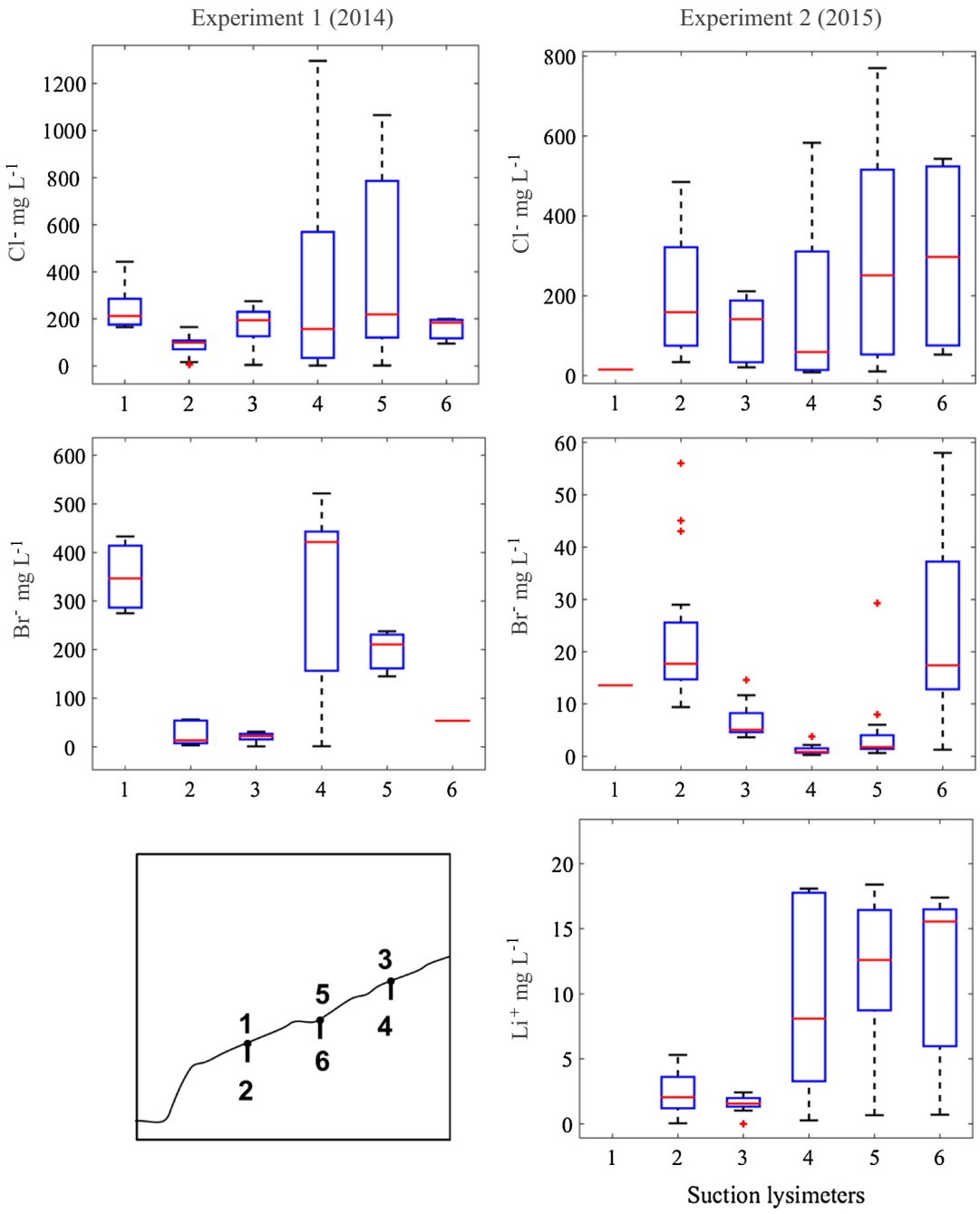

Fig. 5. Box plots showing the range of concentrations of each tracer during Experiment 1 (plots on the left) and Experiment 2 (plots on the right). On each box, the central red mark is the median, the edges of the box are the 25th and 75th percentiles, whilst the black sides show the 5th and 95th percentiles. Red crosses indicate outliers (difference >3 standard deviations). (For interpretation of the references to colour in this figure legend, the reader is referred to the web version of this article.)

4.5.3. Celerity estimated with MICS

Celerity responses on 02/04/2014, using both 50–65 cm depth VWC values and MICS values estimated using different grouping criteria, are shown in Table 4. In both VWC and MICS estimates the lower part of the plot (S1) has lower estimates of celerity than the middle (S2) and top part (S3) (Table 4). The averaged values for MICS are 1761 ± 281 (S3), 986 ± 215 (S2), and 257 ± 172 (S1) mm h^{-1}. VWC-derived average estimates of celerities are 921 ± 76 (S3), 788 ± 112 (S2) and 412 ± 30 mm h^{-1} (S1). VWC-derived estimates show slower celerities with respect to MICS-derived estimates in the case of the top (S3) and middle (S2) locations (Table 4). The bottom site (S1) has an opposite pattern: MICS estimates are lower than VWC ones.

4.5.4. Change in water-filled porosity

The apparent porosity was calculated at the three time steps following the tracer injection and for each grouping criteria. The lower range of porosities observed for time step (b) is between 1.6% (60% criterion) and 4.7% for the 100% criterion. Time step (c) ranges between 3.3% (60% criterion) and 12.0% (the maximum value, for 100%) and time step (d) has intermediate values, between 3.4% (60%) and 10.4 (100%). Only one value exceeded 10%. In the same event, the VWC increment was on average 5.7% at 65 cm depth. Taking into account all the sprinkling days of both experiments, the VWC increment was on average 44.9% at 10 cm depth and 7.9% at 65 cm depth.

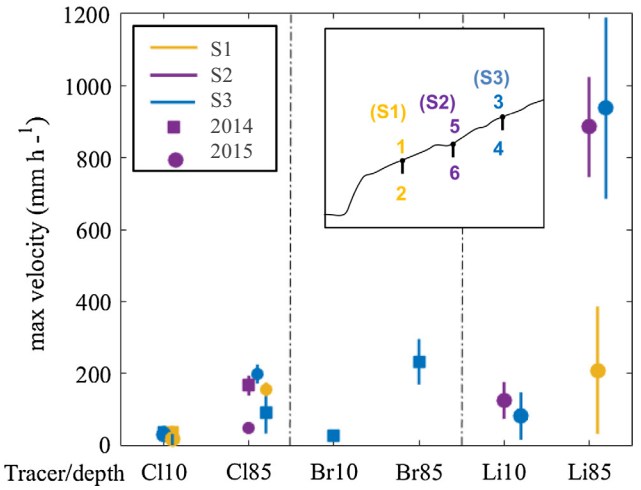

Fig. 6. Range of maximum velocities (y axis) estimated from tracer concentrations at position S1 (yellow), S2 (violet) and S3 (light blue), expressed as mm h^{-1}. Each value is expressed as a range and refers to the detection of the tracers in the sampled water. The node, squared for 2014 samples and round for 2015 samples, indicates the average value. (For interpretation of the references to colour in this figure legend, the reader is referred to the web version of this article.)

5. Discussion

5.1. A predominantly vertical flux direction

It is known from other studies in the Weierbach catchment that subsurface lateral flows contribute to seepage into the riparian areas (Martínez-Carreras et al., 2015; Wrede et al., 2015). The flows on the experimental plot, just 40 m from the stream were, however, predominantly vertical, even after applying large amounts of water. In fact, low volumes of flow reached the trench during the experiments (respectively 0.03% in Experiment 1 and 0.08% in Experiment 2), meaning that most of the water was infiltrating to deeper layers. The near absence of lateral flow during both experiments indicated a strong vertical flow preference. This was consistent over all experiments and under natural rainfall conditions. The small amount of flow at the trench occurred only under the highest rainfall intensities (above 15 mm h^{-1}), and was sporadic. The two wells located at the base of the plot did not detect any saturation during the experiment, showing that the percolation of the sprinkled water must have gone deeper before generating any consistent lateral flow downslope. Any downslope flow is therefore expected to be lower than their depth (2 and 2.40 m from the forest road surface).

The average value of VWC-based celerity in the deep WCR probes (707 ± 234 mm h^{-1}), point-based, was lower than the average value of celerity derived from MICS (971 ± 625 mm h^{-1}) (Table 4). Wetting front measurements were in close agreement with one another, despite the different time steps of the celerity estimates, from 15 min for the TDR probes, to 105 min for the time-lapse ERT. This suggests that MICS methodology applied to time-lapse ERT provided a suitable estimate of flow movement through the soil profile under the conditions observed here.

MICS helped to identify the lower infiltration rate at the bottom of the plot (Fig. 10). Corroborating this behaviour, the deeper WCR probe located at the bottom site in the plot consistently reacted with a longer time lag than the others, and therefore had a value of celerity only half that of the upper sites (Table 4). The reason for this could depend on changes in permeability, possibly linked to disruption during the construction of the forest road, causing a different pattern of infiltration in the lower plot. Moreover, the lower part of the plot received somewhat lower sprinkling intensities, in part due to a deliberate decision to avoid water falling on the roof of the trench.

MICS results showed no expansion in the downslope direction of the infiltration plume at the three time steps (Fig. 10): the movement of water through the soil cannot be detected with MICS at depths further than 2–3 m. Our results on *in situ* measurements

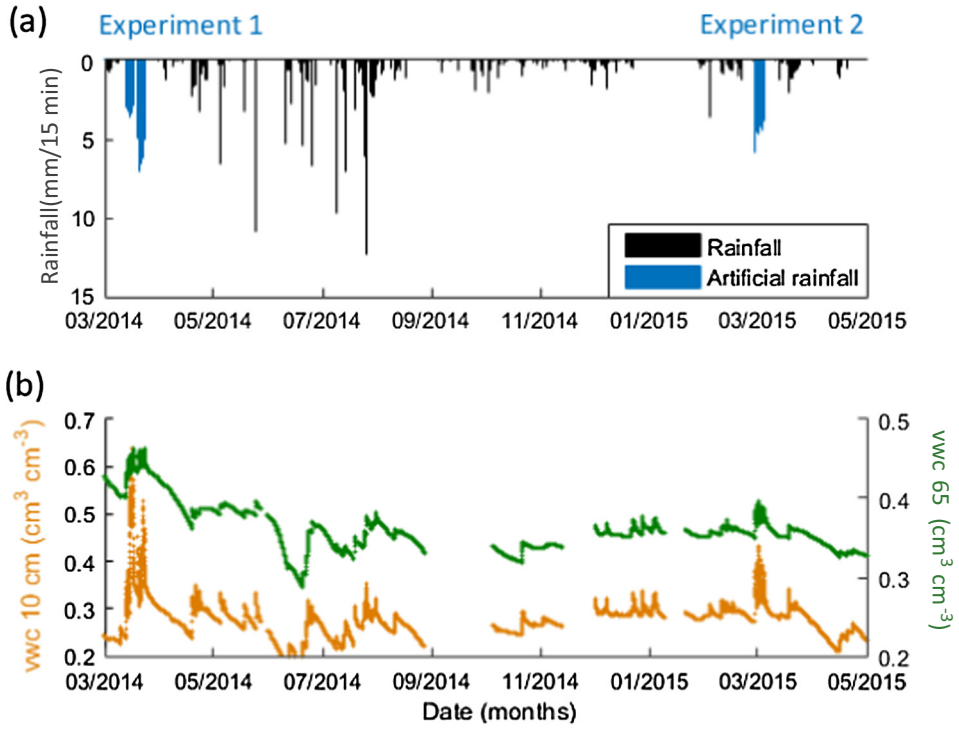

Fig. 7. (a) Time series of rainfall for the period March 2014–May 2015 including the 2 experimental periods. (b) Time series of averaged VWC, at 10 cm and 50–65 cm depth.

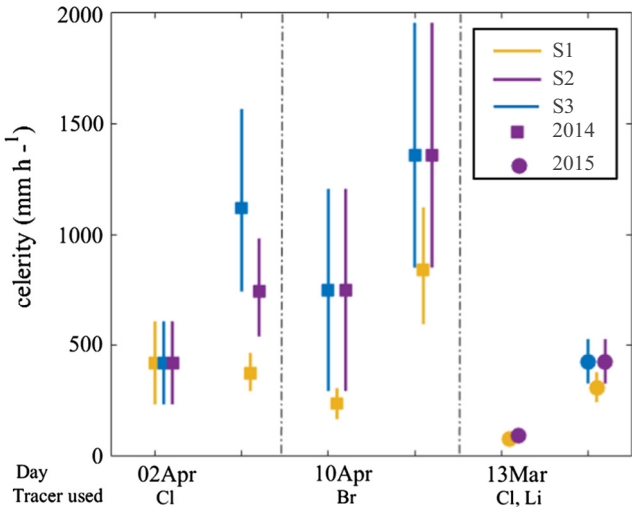

Fig. 8. Celerities estimated from VWC data expressed as mm h^{-1}. Each value of celerity refers to the start of response in terms of VWC at each location. For each day, the values on the left refer to the 10 cm probes, while the values on the right refer to the 50–65 cm depth probes.

(Section 4.2) showed that there is fine-scale variability in the soil structure, and that fine-scale preferential flow is not captured by the coarser resolution of the MICS methodology (Fig. 10). MICS could not therefore be used to draw clear conclusions on lower boundaries for generation of lateral flow. This is partly due to the sensitivity of the ERT method, which is decreasing with depth. On the other hand, MICS requires a high resistivity contrast between the electrically conductive infiltration and the surrounding medium. Despite the very conductive salt tracer solution used (Section 4.5.1), the physical properties of the bedrock below 2.50 m depth, are responsible for a highly conductive pre-sprinkling signal (lower contrast with the surrounding medium), therefore disrupting the capability of MICS to detect infiltration pathways.

The highly permeable material, on which the soil is developing (Section 2), is responsible for the strong prevalent vertical direction of flow through the subsurface. In turn, the subsurface topography is likely controlling lateral flow generation. Although not observed, it is hypothesized that, below 2 m depth, where the slate can still be infiltrated by water (as discussed by Juilleret et al., 2016), more consistent lateral flow takes place.

5.2. Combining celerity and velocity to detect preferential flow

Maximum velocities, estimated by initial tracer detection in suction lysimeter samples, were tracer-dependent and on average 109 ± 89 mm h^{-1} for Cl^-, 178 ± 199 mm h^{-1} for Br^-, and 604 ± 611 mm h^{-1} for Li^+ (averaged from Fig. 6). The observed high variability between maximum velocities of different tracers indicates a complex pattern of movement of tracers through the soil.

In Fig. 3 we showed how the faster velocity can coincide with the wetting front but has an upper limit of the celerity (i.e. it can be equal to the celerity but not higher, unless detected earlier in lysimeters than in the moisture response, Section 3.3). At most of the measurement points and times, celerities were quicker than maximum velocities (Figs. 6 and 8). Only on March 13th the maximum velocities (indicated by the tracer arrivals) were faster than the celerities (as indicated by changes in VWC) on average of 0.2% at 10 cm depth, and 2.6% at the deeper probes (but in location S2 celerities were still higher than velocities). For the other days, celerities were on average 2.7% higher than velocities at 10 cm depth and 6.4% at the deeper probes.

This "paradoxical" behaviour could be explained by intermittent and spatially localised preferential pathways as macropore flow, likely linked to roots, or channelled via horizontally layered stones. In this interpretation, preferential flow would need to deliver some solution to the suction lysimeters before the WCR probe located above them could detect wetting.

Even if differences between velocities and celerities may be intensified by the lower time resolution of the suction lysimeters sampling with respect to the WCR, and the depth at which celeri-

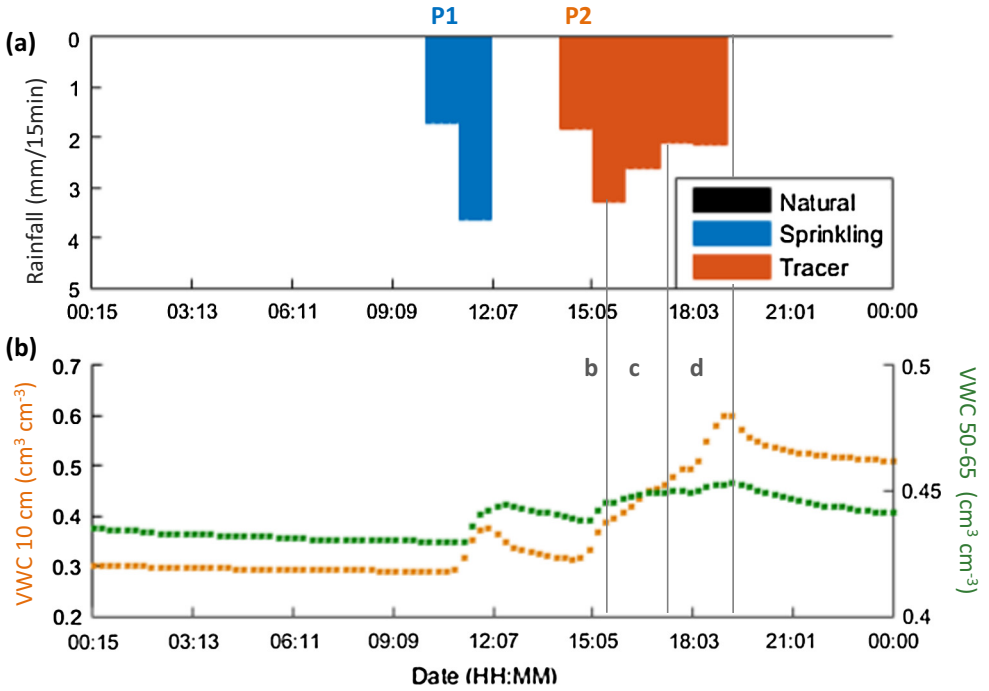

Fig. 9. Time series of artificial rainfall (a) and averaged value of VWC response (b) on Day 3 of Experiment 1. Vertical lines show the time step of the time-lapse ERT profiles that followed the start of sprinkling of the salt solution. In grey, letters indicate the time step corresponding to Fig. 10.

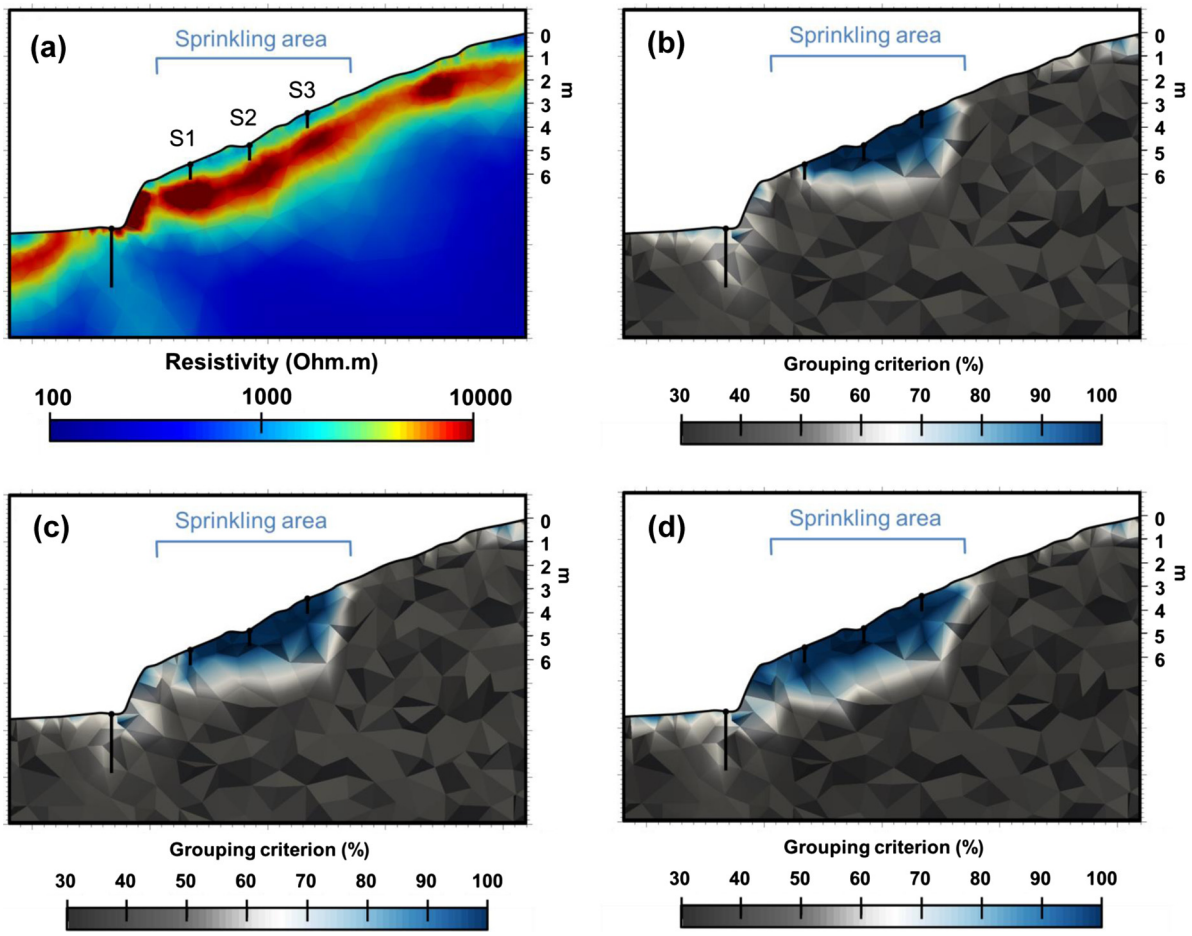

Fig. 10. (a) Results of a standard inversion of the initial time step before salt sprinkling experiment. (b, c and d) Visualisation of the results of the MICS strategy applied to the three time steps following the starting of the tracer experiment, respectively 70, 175 and 280 min after start of salt sprinkling. The infiltration bulb at each time step is characterised by blue to white-coloured pixels for the 100–60% grouping criterion. Grey-coloured areas correspond to criteria lower than 60%.

Table 4
Celerities estimated using the VWC data and the correspondent celerity estimated using MICS. **Bold**: average values. All the estimates are expressed in mm h^{-1}.

	Celerities (mm h^{-1})				
	VWC	MICS			
Position		70%	80%	90%	**Average**
S3	921 ± 76	1929	1714	1371	**1671 ± 281**
S2	788 ± 112	1200	986	771	**986 ± 215**
S1	412 ± 30	429	257	86	**257 ± 172**
Average	**707 ± 234**				**971 ± 625**

ties are measured (50–65 cm depth for WCR probes and 80–90 cm for suction lysimeters), there were other indications of a preferential flow type of process. The apparent porosity ε_a calculated from MICS at the three time steps following the tracer injection (Experiment 1) ranged between 1.4% and 12%. The average apparent increase in VWC in the wetted volume is therefore relatively small, particularly in the deeper WCR probes (Section 4.5.4). Given the rates of infiltration applied and the ε_a values, this suggests fast and possibly preferential flow pathways.

Finally, a preferential type of flow is corroborated by trench flow characteristics. Trench flow main characteristics were: [i] intermittent flow during Experiment 2, even in presence of relatively constant rainfall; [ii] a very high variability in the concentration of tracers at the trench, with differences of more than 4 standard deviations between tracer concentrations of samples taken 5 min apart at same depth in the trench. Sporadic and spatially restricted outflow was also described by Kim et al. (2005), in a hillslope characterised by shallow soils formed in colluvium and glacial till. At our site, the highly variable concentrations of the intermittent flow to the trench had all lower concentrations than sprinkled concentrations.

Since trench concentrations are lower than the applied concentrations, this indicates that some displacement of stored water takes place even given fast preferential flow response. These direct flows to the trench, not subject to as much mixing as in the in the suction lysimeters (due to the difference in the sampling interval, lower for the suction lysimeters), are therefore not just a simple preferential flow of applied water, but a more complex flow dynamic. The imbricate structure of the coarse clasts, oriented parallel to the slope, could be driving the flow laterally (as proposed

by Heller and Kleber, 2016, on periglacial cover beds), favouring a preferential flow network.

5.3. Tracer dynamics

Experiment 2 showed lower celerities than Experiment 1 (Fig. 8), despite input intensities of a similar magnitude of Experiment 1, step 2 (Table 2). The lower values of celerities might be due to compaction of the soil around the probes over the period between the experiments, but could also be a consequence of change to the soil structure as a result of chemical processes following the addition of the tracer solution during Experiment 1 (Klaus et al., 2014; Wendroth et al., 2011).

Indeed, applying large amounts of salt to the soil surface can generate tracer-dependent changes in the soil structure (Perkins et al., 2011; Yalamanchali, 2012; Yousefi et al., 2014). High concentrations of cations, particularly K^+ and Na^+, are known to be responsible for a decrease in permeability and a reduced hydraulic conductivity (Rengasamy and Olsson, 1991). Due to the experiments, Na^+ had an average value of 174.00 ± 80.00 mg L^{-1}, and concentrations of K^+ were also raised to an average of 27.00 ± 10.00 mg L^{-1}.

Values of maximum velocities were very different across tracers, indicating strong dependence on the tracer used. Cl^- maximum velocities were lower than both Br^- and Li^+, while Li^+ had the highest maximum velocities (Fig. 6).

Our interpretation depends on comparing celerity responses with conservative tracer responses. The non-uniformity of the rainfall intensity surely has an influence on the velocity/celerity relationship (Beven, 2012). Biogeochemical interactions and sorption are considered as the primary reasons for different tracer behaviour.

Understanding soil-tracer interactions is extremely difficult. In an effort to understand the differences in the velocities measured during the experiments, we briefly outline the processes that might affect tracer movement:

i. *Anion exclusion.* Cl^- and particularly Br^- can be transported through pores slightly faster than water molecules, due to the anion exclusion phenomenon, linked to the repulsion of anions from the negatively charged soil particles (Flury and Wai, 2003).
ii. *Chlorination.* The soil organic matter can instantaneously trap Cl^- in the upper soil layer (which is enriched in organic matter) (Bastviken et al., 2007).
iii. *Anion retardation.* Salt addition affected the dominant charge of the soil. The strong content of Na^+ and K^+ could have given a positive charge to the soil, generating the conditions for anion retardation (due to sorption, see Sposito, 1989). In support of this hypothesis, salt aggregates had been observed on the soil surface (primarily NaCl and KCl).

Chlorination may have slowed down Cl^- respect to Br^-, and some combination of factors may have accelerated the passage of Li^+ explaining the higher maximum velocity values observed in Fig. 6. After one year of natural rainfall, any residual effect of [i], [ii] and [iii] could have been mitigated, though we do not have direct evidence to support or refute this. We have no particular evidence that any of these processes might prevail over simple conservative transport, nor it was not the aim of this study to explore such chemical processes.

Additional information about mixing and tracer presence in the soil is provided by the multi-parameter sensor located in the middle of the plot (Fig. 4). The salt sprinkled during Experiment 1 remained in the soil long after the experiment (Fig. 4). The strong signal of EC in response to natural rainfall events shows remobilisation of the salt stored in the soil matrix, particularly during the heavy rainfall events in summer of 2014 (Fig. 4a). Soil analysis performed in autumn 2014 (i.e. 6 months after Experiment 1) strengthens this point: there were significant amounts of Cl^- and Br^- stored in the soil, to be remobilised during later rainfall events (Section 4.2). In the same way, Br^- was found in all the samples collected during Experiment 2, both at the trench and in the suction lysimeters (Section 4.2).

Chemical transport processes were present at the site well after the experiment. Remobilisation was peaking at the same time as the VWC peaks, therefore suggesting a system limited by transport. The salt was finally depleted towards the end of the summer, after a total of 500 mm of natural rainfall had infiltrated. Rainfall events following the summer period (additional 250 mm) did not cause the same release of tracers. The system was therefore limited by supply in this period (Fig. 4b), even though there was still residual tracer within the soil matrix suggested by the suction lysimeter samples (Section 4.2). In March 2015 a strong response was observed due to the last application of tracer (Fig. 4c).

6. Conclusions

The relationship between tracer velocities and wave or wetting front celerities is essential for understanding the complexity of flow from hillslopes to the stream. No experimental studies have yet connected estimates of the maximum velocity and wetting front derived from state-of-the-art experimental techniques. To fill this gap, the maximum velocity and the celerity responses were explored in a plot located in the Weierbach catchment, where subsurface flows are known to contribute to riparian zone wetness and streamflows. Maximum tracer velocities and wetting front celerities were determined at plot scale using a three-fold monitoring protocol (including artificial tracers, time domain reflectrometry and time-lapse electrical resistivity tomography).

This study demonstrated the potential of different measurement approaches in facilitating the interpretation and quantification of infiltrating water flows. This work demonstrated that MICS, can help to understand wetting front dynamics, but it cannot capture local wetness patterns/lateral flow. The ERT method, as used here, does not detect wetting fronts or tracer transport at depths further than 2–3 m depending on the grouping criteria, due in part to the coarse resolution and in part to the characteristics of the bedrock (in particular its low porosity and resistivity).

It was found that tracer-specific properties influenced the response in terms of maximum velocity. In particular, Li^+, the last tracer used, reached the measurement points with velocities much higher than Br^-, and both were detected quicker than Cl^-, the first tracer to be employed and the more abundant in the input water (and the only one being naturally present in this soil). Moreover, tracers and soil compression during Experiment 1 potentially altered the soil structure and may have influenced the celerity estimates. A more extensive soil survey is being undertaken to understand tracer interactions at this soil.

No lateral flow was observed in the trench apart from a few preferential pathways. Preferential flow processes were indicated by three different results: [i] maximum velocities apparently greater than celerities observed during experiment 2, [ii] scattered trench flow response with highly variable tracer concentrations and [iii] very low range of apparent porosity calculated using both MICS and deep VWC.

Maximum velocity information proved to be essential to understand flow dynamics in response to sprinkling, while information on the wetting front alone would have missed important processes. This analysis demonstrates that measuring tracer velocities was of greater importance for understanding hillslope

dynamics than capturing only celerity information. It also demonstrates the value of tracer data, soil moisture and ERT data at high time resolution, for interpreting hillslope dynamics. The results described in this study pose the basis for integrating in a simple way measures of celerity and maximum velocity into hydrological studies. The conditions required for the lateral connectivity to be present remain unknown and are the focus of further analysis.

Acknowledgments

Research funded by National Research Fund of Luxemburg (FNR) core project ECSTREAM (C12/SR/40/8854) and the Luxembourg Institute for Science and Technology (LIST). The authors would like to thank all the colleagues that helped during the long field campaigns: Jean François Iffly, Giovanni Corato, Jay Frentress, Cristina Moragues Quiroga, Michael Schwab, Carlos Eduardo Wetzel, Núria Martínez Carreras, Marta Antonelli, Olivier Faber, Renaud Hostache, Jerôme Juilleret and Aina Martínez Useros. François Barnich and Delphine Collard are thanked for the chemical analysis. Jay Frentress and Rémi Clement are thanked for comments on an earlier version of the manuscript.

References

Athanasiou, E.N., Tsourlos, P.I., Papazachos, C.B., Tsokas, G.N., 2007. Combined weighted inversion of electrical resistivity data arising from different array types. J. Appl. Geophys. 62, 124–140.

Audebert, M., Clément, R., Moreau, S., Duquennoi, C., Loisel, S., Touze-foltz, N., 2016. Understanding leachate flow in municipal solid waste landfills by combining time-lapse ERT and subsurface flow modelling – Part I: Analysis of infiltration shape on two different waste deposit cells. Waste Manage. http://dx.doi.org/10.1016/j.wasman.2016.04.006.

Audebert, M., Clément, R., Touze-Foltz, N., Günther, T., Moreau, S., Duquennoi, C., 2014. Time-lapse ERT interpretation methodology for leachate injection monitoring based on multiple inversions and a clustering strategy (MICS). J. Appl. Geophys. 111, 320–333. http://dx.doi.org/10.1016/j.jappgeo.2014.09.024.

Bastviken, D., Thomsen, F., Svensson, T., Karlsson, S., Sandén, P., Shaw, G., Matucha, M., ÖBerg, G., 2007. Chloride retention in forest soil by microbial uptake and by natural chlorination of organic matter. Geochim. Cosmochim. Acta 71, 3182–3192. http://dx.doi.org/10.1016/j.gca.2007.04.028.

Benettin, P., Kirchner, J.W., Rinaldo, A., Botter, G., 2015. Modeling chloride transport using travel time distributions at Plynlimon, Wales. Water Resour. Res. 51, 3259–3276. http://dx.doi.org/10.1002/2014WR016600.

Bergstrom, A., Mcglynn, B., Mallard, J., Covino, T., 2016. Watershed structural influences on the distributions of stream network water and solute travel times under baseflow conditions. Hydrol. Process. http://dx.doi.org/10.1002/hyp.10792.

Beven, K., 2012. The Primer, Rainfall-Runoff Modelling. John Wiley & Sons, Ltd.. http://dx.doi.org/10.1002/9781119951001.

Beven, K.J., 2010. Preferential flows and travel time distributions: defining adequate hypothesis tests for hydrological process models. Hydrol. Process. 24, 1537–1547. http://dx.doi.org/10.1002/hyp.7718.

Beven, K.J., 1989. Interflow, Unsaturated Flow in Hydrologic Modeling: Theory and Practice. Kluwer Academic Publ., Dordrecht.

Binley, A., Kemna, A., 2005. Electrical methods. In: Hubbard, R. (Ed.), Hydrogeophysics. Springer, pp. 129–156.

Botter, G., Bertuzzo, E., Rinaldo, A., 2010. Transport in the hydrologic response: travel time distributions, soil moisture dynamics, and the old water paradox. Water Resour. Res. 46. http://dx.doi.org/10.1029/2009WR008371.

Cassiani, G., Bruno, V., Villa, A., Fusi, N., Binley, A.M., 2006. A saline trace test monitored via time-lapse surface electrical resistivity tomography. J. Appl. Geophys. 59, 244–259. http://dx.doi.org/10.1016/j.jappgeo.2005.10.007.

Cassiani, G., Godio, A., Stocco, S., Villa, A., Deiana, R., Frattini, P., Rossi, M., 2009. Monitoring the hydrologic behaviour of a mountain slope via time-lapse electrical resistivity tomography. Near Surf. Geophys. 7, 475–486. http://dx.doi.org/10.3997/1873-0604.2009013.

Chambers, J.E., Wilkinson, P.B., Uhlemann, S., Sorensen, J.P.R., Roberts, C., Newell, A. J., Ward, W.O.C., Binley, A., Williams, P.J., Gooddy, D.C., Old, G., Bai, L., 2014. Derivation of lowland riparian wetland deposit architecture using geophysical image analysis and interface detection. Water Resour. Res. 50, 5886–5905. http://dx.doi.org/10.1002/2012WR013085.

Clément, R., Oxarango, L., Descloitres, M., 2011. Contribution of 3-D time-lapse ERT to the study of leachate recirculation in a landfill. Waste Manage. 31, 457–467.

Dahlin, T., 2001. The development of DC resistivity imaging techniques. Comput. Geosci. 27, 1019–1029.

Dahlin, T., Zhou, B., 2004. A numerical comparison of 2D resistivity imaging with 10 electrode arrays. Geophys. Prospect. 52, 379–398.

Daily, W., Ramirez, A., LaBrecque, D., Nitao, J., 1992. Electrical resistivity tomography of vadose water movement. Water Resour. Res. 28, 1429–1442. http://dx.doi.org/10.1029/91wr03087.

Dalton, F.N., Herkelrath, W.N., Rawlins, D.S., Rhoades, J.D., 1984. Time-domain reflectometry: simultaneous measurement of soil water content and electrical conductivity with a single probe. Science 224, 989–990. http://dx.doi.org/10.1126/science.224.4652.989.

Davies, J., Beven, K., Nyberg, L., Rodhe, A., 2011. A discrete particle representation of hillslope hydrology: hypothesis testing in reproducing a tracer experiment at Gårdsjön, Sweden. Hydrol. Process. 25, 3602–3612. http://dx.doi.org/10.1002/hyp.8085.

Davies, J., Beven, K., Rodhe, A., Nyberg, L., Bishop, K., 2013. Integrated modeling of flow and residence times at the catchment scale with multiple interacting pathways. Water Resour. Res. 49, 4738–4750. http://dx.doi.org/10.1002/wrcr.20377.

Descloitres, M., Ribolzi, O., Troquer, Y.Le., Thiebaux, J.P., 2008. Study of water tension differences in heterogeneous sandy soils using surface ERT. J. Appl. Geophys. 64, 83–98.

Fenicia, F., Kavetski, D., Savenije, H.H.G., Clark, M.P., Schoups, G., Laurent, P., Freer, J., 2013. Catchment properties, function, and conceptual model representation: is there a correspondence? doi:http://dx.doi.org/10.1002/hyp.9726.

Flury, M., Papritz, A., 1993. Bromide in the natural environment: occurrence and toxicity. J. Environ. Qual. 22, 743–758.

Flury, M., Wai, N.N., 2003. Dyes as tracers for vadose zone hydrology. Rev. Geophys. 41, 1002. http://dx.doi.org/10.1029/2001RG000109.

Graham, C.B., McDonnell, J.J., 2010. Hillslope threshold response to rainfall: (2) Development and use of a macroscale model. J. Hydrol. 393, 77–93. http://dx.doi.org/10.1016/j.jhydrol.2010.03.008.

Graham, C.B., Woods, R.A., McDonnell, J.J., 2010. Hillslope threshold response to rainfall: (1) a field based forensic approach. J. Hydrol. 393, 65–76. http://dx.doi.org/10.1016/j.jhydrol.2009.12.015.

Günther, T., Rücker, C., Spitzer, K., 2006. Three-dimensional modelling and inversion of dc resistivity data incorporating topography – II. Inversion. Geophys. J. Int. 166, 506–517. http://dx.doi.org/10.1111/j.1365-246X.2006.03011.x.

Haga, H., Matsumoto, Y., Matsutani, J., Fujita, M., Nishida, K., Sakamoto, Y., 2005. Flow paths, rainfall properties, and antecedent soil moisture controlling lags to peak discharge in a granitic unchanneled catchment. Water Resour. Res. 41. http://dx.doi.org/10.1029/2005WR004236. n/a–n/a.

Heller, K., Kleber, A., 2016. Hillslope runoff generation influenced by layered subsurface in a headwater catchment in Ore Mountains, Germany. Environ. Earth Sci. 75, 943. http://dx.doi.org/10.1007/s12665-016-5750-y.

Hrachowitz, M., Benettin, P., van Breukelen, B.M., Fovet, O., Howden, N.J.K., Ruiz, L., van der Velde, Y., Wade, A.J., 2016. Transit times-the link between hydrology and water quality at the catchment scale. Wiley Interdiscip. Rev. Water. http://dx.doi.org/10.1002/wat2.1155.

Hrachowitz, M., Savenije, H., Bogaard, T.A., Tetzlaff, D., Soulsby, C., 2013. What can flux tracking teach us about water age distribution patterns and their temporal dynamics? Hydrol. Earth Syst. Sci. 17, 533–564. http://dx.doi.org/10.5194/hess-17-533-2013.

Jackson, R.C., Du, E., Klaus, J., Griffiths, N.A., Bitew, M., McDonnell, J.J., 2016. Interactions among hydraulic conductivity distributions, subsurface topography, and transport thresholds revealed by a multi-tracer hillslope irrigation experiment. Water Resour. Res., 2–43 http://dx.doi.org/10.1002/2015WR018364.

Juilleret, J., Dondeyne, S., Vancampenhout, K., Deckers, J., Hissler, C., 2016. Mind the gap: a classification system for integrating the subsolum into soil surveys. Geoderma. http://dx.doi.org/10.1016/j.geoderma.2015.08.031.

Juilleret, J., Iffly, J.F., Pfister, L., Hissler, C., 2011. Remarkable Pleistocene periglacial slope deposits in Luxembourg (Oesling): pedological implication and geosite potential. Bull. Soc. Nat. Luxemb. 112, 125–130.

Kim, H.J., Sidle, R.C., Moore, R.D., 2005. Shallow lateral flow from a forested hillslope: influence of antecedent wetness. Catena 60, 293–306. http://dx.doi.org/10.1016/j.catena.2004.12.005.

Kirchner, J.W., 2016. Aggregation in environmental systems – Part 1: Seasonal tracer cycles quantify young water fractions, but not mean transit times, in spatially heterogeneous catchments. Hydrol. Earth Syst. Sci. 20, 279–297. http://dx.doi.org/10.5194/hess-20-279-2016.

Kirchner, J.W., 2006. Getting the right answers for the right reasons: linking measurements, analyses, and models to advance the science of hydrology. Water Resour. Res. 42, W03S04. http://dx.doi.org/10.1029/2005wr004362.

Kirchner, J.W., 2003. A double paradox in catchment hydrology and geochemistry. Hydrol. Process. 17, 871–874. http://dx.doi.org/10.1002/hyp.5108.

Klaus, J., Zehe, E., Elsner, M., Palm, J., Schneider, D., Schröder, B., Steinbeiss, S., Van Schaik, L., West, S., 2014. Controls of event-based pesticide leaching in natural soils: a systematic study based on replicated field scale irrigation experiments. J. Hydrol. 512, 528–539. http://dx.doi.org/10.1016/j.jhydrol.2014.03.020.

Laine-Kaulio, H., Backnäs, S., Karvonen, T., Koivusalo, H., McDonnell, J.J., 2014. Lateral subsurface stormflow and solute transport in a forested hillslope: a combined measurement and modeling approach. Water Resour. Res. 50, 8159–8178. http://dx.doi.org/10.1002/2014wr015381.

Loke, M.H., Barker, R.D., 1996. Rapid least-squares inversion of apparent resistivity pseudosections using a quasi-Newton method. Geophys. Prospect. 44, 131–152.

Martínez-Carreras, N., Hissler, C., Gourdol, L., Klaus, J., Juilleret, J., François Iffly, J., Pfister, L., 2016. Storage controls on the generation of double peak hydrographs in a forested headwater catchment. J. Hydrol. http://dx.doi.org/10.1016/j.jhydrol.2016.10.004.

Martínez-Carreras, N., Wetzel, C.E., Frentress, J., Ector, L., McDonnell, J.J., Hoffmann, L., Pfister, L., 2015. Hydrological connectivity as indicated by transport of diatoms through the riparian–stream system. Hydrol. Earth Syst. Sci. Discuss. 12, 2391–2434. http://dx.doi.org/10.5194/hessd-12-2391-2015.

McDonnell, J.J., Beven, K., 2014. Debates—the future of hydrological sciences: a (common) path forward? A call to action aimed at understanding velocities, celerities and residence time distributions of the headwater hydrograph. Water Resour. Res. 50, 5342–5350. http://dx.doi.org/10.1002/2013wr015141.

McDonnell, J.J., Sivapalan, M., Vaché, K., Dunn, S., Grant, G., Haggerty, R., Hinz, C., Hooper, R., Kirchner, J., Roderick, M.L., Selker, J., Weiler, M., 2007. Moving beyond heterogeneity and process complexity: a new vision for watershed hydrology. Water Resour. Res. 43. http://dx.doi.org/10.1029/2006WR005467.

McGlynn, B.L., McDonnel, J.J., Brammer, D.D., 2002. A review of the evolving perceptual model of hillslope flowpaths at the Maimai catchments, New Zealand. J. Hydrol. 257.

McNeil, V.H., Cox, M.E., 2000. Relationship between conductivity and analysed composition in a large set of natural surface-water samples, Queensland, Australia. Environ. Geol. 39, 1325–1333. http://dx.doi.org/10.1007/s002549900033.

Nguyen, F., Garambois, S., Jongmans, D., Pirard, E., Loke, M.H., 2005. Image processing of 2D resistivity data for imaging faults. J. Appl. Geophys. 57, 260–277.

Nickus, U., 2001. Ion chromatographic determination of lithium at trace level concentrations: application to a tracer experiment in a high-mountain lake. J. Chromatogr. A 920, 201–204.

Park, S., 1998. Fluid migration in the vadose zone from 3-D inversion of resistivity monitoring data. Geophysics 63, 41–51.

Perkins, K., 2011. Measurement and Modeling of Unsaturated Hydraulic Conductivity, Hydraulic Conductivity – Issues, Determination and Applications.

Perkins, K.S., Nimmo, J.R., Rose, C.E., Coupe, R.H., 2011. Field tracer investigation of unsaturated zone flow paths and mechanisms in agricultural soils of northwestern Mississippi, USA. J. Hydrol. 396, 1–11. http://dx.doi.org/10.1016/j.jhydrol.2010.09.009.

Persson, M., 1997. Soil solution electrical conductivity measurements under transient conditions using time domain reflectometry. Soil Sci. Soc. Am. J. 61, 997–1003.

Rengasamy, P., Olsson, K., 1991. Sodicity and soil structure. Aust. J. Soil Res. 29, 935. http://dx.doi.org/10.1071/SR9910935.

Rinaldo, A., Beven, K.J., Bertuzzo, E., Nicotina, L., Davies, J., Fiori, A., Russo, D., Botter, G., 2011. Catchment travel time distributions and water flow in soils. Water Resour. Res. 47. http://dx.doi.org/10.1029/2011WR010478. n/a–n/a.

Scientific, C., 2011. Instruction Manual, CS650 and CS655 Water Content Reflectometers.

Siosemarde, M., Kave, F., Pazira, E., Sedghi, H., Ghaderi, S.J., 2010. Determine of constant coefficients to relate total dissolved solids to electrical conductivity. Aust. J. Soil Res. 4, 258–260.

Slater, L., Binley, A., Versteeg, R., Cassiani, G., Birken, R., Sandberg, S., 2002. A 3D ERT study of solute transport in a large experimental tank. J. Appl. Geophys. 49, 211–229.

Sposito, G., 1989. The Chemistry of Soils. Oxford Univ. Press, New York.

Telford, W.M., Geldart, L.P., Sheriff, R.E., 1990. Applied Geophysics. Cambridge Univ..

Topp, G.C., Davis, J.L., Annan, A.P., 1980. Electromagnetic determination of soilwater content: measurements in coaxial transmission lines. Water Resour. Res. 16, 574–582.

Travelletti, J., Sailhac, P., Malet, J.-P., Grandjean, G., Ponton, J., 2012. Hydrological response of weathered clay-shale slopes: water infiltration monitoring with time-lapse electrical resistivity tomography. Hydrol. Process. 26, 2106–2119. http://dx.doi.org/10.1002/hyp.7983.

Tsourlos, P.I., Ogilvy, R.D., 1999. An algorithm for the 3-D inversion of tomographic resistivity and induced polarisation data: preliminary results. J. Balk. Geophys. Soc. 2, 30–45.

Tyner, J.S., Wright, W.C., Yoder, R.E., 2007. Identifying long term preferential and matrix flow recharge at the field scale. Trans. Am. Soc. Agric. Biol. Eng. 50, 2001–2006.

Valipour, M., 2012. Sprinkle and trickle irrigation system design using tapered pipes for pressure loss adjusting. J. Agric. Sci. 4, 125–133. http://dx.doi.org/10.5539/jas.v4n12p125.

Valipour, M., Singh, V.P., 2016. Global experiences on wastewater irrigation: challenges and prospects. In: Maheshwari, B., Singh, V.P., Thoradeniya, B. (Eds.), Balanced Urban Development: Options and Strategies for Liveable Cities. Springer Open, Water Science and Technology Library. http://dx.doi.org/10.1007/978-3-319-28112-4.

Vereecken, H., Huisman, J.A., Franssen, H.J.H., Brüggemann, N., Bogena, H.R., Kollet, S., Javaux, M., van der Kruk, J., Vanderborght, J., 2014. Soil hydrology: recent methodological advances, challenges, and perspectives. Water Resour. Res. 51, 2616–2633. http://dx.doi.org/10.1016/0022-1694(68)90080-2.

Wagner, G.H., 1962. Use of porous ceramic cups to sample soil water within the profile. Soil Sci. 94, 379–386.

Ward, W.O.C., Wilkinson, P.B., Chambers, J.E., Oxby, L.S., Bai, L., 2014. Distribution-based fuzzy clustering of electrical resistivity tomography images for interface detection. Geophys. J. Int. 197, 310–321. http://dx.doi.org/10.1093/gji/ggu006.

Weihermüller, L., Kasteel, R., Vanderborght, J., Pütz, T., Vereecken, H., 2005. Soil water extraction with a suction cup. Vadose Zone J. 4, 899. http://dx.doi.org/10.2136/vzj2004.0156.

Weihermüller, L., Siemens, J., Deurer, M., Knoblauch, S., Rupp, H., Göttlein, A., Pütz, T., 2007. In situ soil water extraction: a review. J. Environ. Qual. 36, 1735–1748. http://dx.doi.org/10.2134/jeq2007.0218.

Wendroth, O., Vasquez, V., Matocha, C.J., 2011. Field experimental approach to bromide leaching as affected by scale-specific rainfall characteristics. Water Resour. Res. 47, W00L03. http://dx.doi.org/10.1029/2011WR010650.

Wienhöfer, J., Germer, K., Lindenmaier, F., Färber, A., Zehe, E., 2009. Applied tracers for the observation of subsurface stormflow at the hillslope scale. Hydrol. Earth Syst. Sci. 13, 1145–1161.

Wienhöfer, J., Zehe, E., 2014. Predicting subsurface stormflow response of a forested hillslope – the role of connected flow paths. Hydrol. Earth Syst. Sci. 18, 121–138. http://dx.doi.org/10.5194/hess-18-121-2014.

WRB, I.W.G., 2015. World Reference Base for Soil Resources 2015: international soil classification system for naming soils and creating legends for soil maps. In: World Soil Resources Reports. FAO, Rome.

Wrede, S., Fenicia, F., Martínez-Carreras, N., Juilleret, J., Hissler, C., Krein, A., Savenije, H.H.G., Uhlenbrook, S., Kavetski, D., Pfister, L., 2015. Towards more systematic perceptual model development: a case study using 3 Luxembourgish catchments. Hydrol. Process. 29, 2731–2750. http://dx.doi.org/10.1002/hyp.10393.

Yalamanchali, R.C., 2012. Lithium, an emerging environmental contaminant, is mobile in the soil-plant system. Lincoln Univ. Digit. Thesis Lincoln Univ., Canterbury, New Zeal.

Yousefi, G., Safadoust, A., Mahboubi, A.A., Gharabaghi, B., Mosaddeghi, M.R., Ahrens, B., Shirani, H., 2014. Bromide and lithium transport in soils under long-term cultivation of alfalfa and wheat. Agric. Ecosyst. Environ. 188, 221–228. http://dx.doi.org/10.1016/j.agee.2014.02.031.

Zehe, E., Sivapalan, M., 2009. Threshold behavior in hydrological systems and geo-ecosystems: manifestations, controls and implications for predictability. Hydrol. Earth Syst. Sci. Discuss. 5, 3247–3312. http://dx.doi.org/10.5194/hessd-5-3247-2008.